

Identification of Astrophysical Black Holes

Sandip K. Chakrabarti

S.N. Bose National Centre for Basic Sciences
JD-Block, Sector-III, Salt Lake, Calcutta 700091, INDIA

March 29, 2021

Abstract

Black holes are by definition *black*, and therefore cannot be directly observed by using electromagnetic radiations. Convincing identification of black holes must necessarily depend on the identification of a very specially behaving matter and radiation which surround them. A major problem in this subject of black hole astrophysics is to quantify the behaviour of matter and radiation close to the horizon. In this review, the subject of black hole accretion and outflow is systematically developed. It is shown that both the stationary as well as the non-stationary properties of the observed spectra could be generally understood by these solutions. It is suggested that the solutions of radiative hydrodynamic equations may produce clear spectral signatures of black holes. Other circumstantial evidences of black holes, both in the galactic centers as well as in binary systems, are also presented.

ACCEPTED FOR PUBLICATION (March 2nd, 1998) IN INDIAN JOURNAL OF PHYSICS (REVIEW SECTION).

1 Introduction

Stellar mass black holes are the end products of stars. After the fuel is exhausted inside a normal star, the core collapses and the supernova explosion occurs. If the mass of the core is lower than, say, $\sim 3M_{\odot}$, the object formed at the center may be a neutron star. Otherwise, it is a black hole. Therefore,

some of the compact binary systems should contain black holes. Similarly, core collapse in the proto-galactic phase could also produce supermassive black holes ($M \sim 10^6$ to $10^9 M_\odot$). In spiral galaxies, the central black holes are less massive (say, $10^{6-7} M_\odot$), while in elliptical galaxies the central black holes are more massive (say, a few times $10^{8-9} M_\odot$).

Astrophysical community generally believes that the black holes should exist because of the solid foundation of the theory of general relativity which predicts them. The problem remains that of identification. Black holes do not emit anything except Hawking radiation, which, for any typical mass of the astrophysical black holes is so cold (typically 60 nano Kelvin for a solar mass black hole, and goes down inversely with increase in mass) that it would be entirely masked by the much hotter microwave background radiation. Classically, black holes are point-like with infinite density and are surrounded by an imaginary one-way membrane called ‘event horizon’ of radius $R_g = 2GM_{BH}/c^2$. Here, G and c are gravitational constant and velocity of light respectively, M_{BH} is the mass of the black hole. R_g is known as the Schwarzschild radius and is roughly equal to 30 kilometers for a $10 M_\odot$ black hole. For a maximally rotating (Kerr) black hole, the radius is half as small. Surrounding matter and radiation are pulled by the black hole only to disappear inside never to be observed again. Not even light, what to talk about matter, can escape to distant observers from regions within the horizon, making it *impossible* to detect a black hole through direct observations. A positive identification must therefore rely on indirect and circumstantial evidences. In fact, the problem of identification of black holes boils down to the identification of surrounding matter which may behave in a ‘funny’ way. We shall quantify the degree of ‘funniness’ as we go along.

In this *review*, we discuss how a black hole could be identified. We first present elementary properties of the spacetime around a black hole and compare them with those of a Newtonian star. We discuss in great length the properties of the global solutions of equations which govern the behaviour of matter. We then show that the observations in the last couple of decades do agree with these properties. Towards the end we make a comparative study of methodologies of black hole detection and present our judgment on the best way to detect black holes.

2 Behaviour of Matter Around a Black Hole: Theoretical Expectations

Generally speaking, we shall use geometrical units where masses, lengths and times are measured in units of mass of the black hole M_{BH} , the Schwarzschild radius of the black hole $r_g = 2GM_{BH}/c^2$ and the light crossing time $t_g = 2GM_{BH}/c^3$ of the black hole respectively. Since this is a review, and some figures of other works with different conventions had to be borrowed, we may use GM_{BH}/c^3 for the length scale for the lengthscale, instead. Radial distances would be generally denoted by r and in component form $x = r$ would be used. Angular momentum would be denoted by l for inviscid flows and λ for viscous flows. We shall mention the choice of units whenever any confusion arises. Sometimes we may revert back to cgs unit when we need to put in numbers.

A few elementary definitions in this context are in order: The process by which matter falls into a black hole or a neutron star (or, to any star, in general) is known as *accretion*. The accretion rate refers to the rate (in units of, e.g., *gms/sec*) at which matter falls into a black hole at a certain radius. For a steady state accretion, this rate is fixed at all radii. Matter usually comes with some angular momentum. A Keplerian distribution of angular momentum is achieved when the centrifugal force of the matter that spirals into the black hole matches with the gravitational force acting on it. If other forces, such as that due to radiation pressure, ion pressure, inertial force etc. are operating, the disk need not be Keplerian.

Followings are the estimates of physical quantities around black holes:

1. *Length scale: r_g .* Physical quantities are expected to have variations in not too smaller than this length. Similarly, if there are perturbations on accretion disks, the size of the perturbations are also of similar length. $r_g \sim 3 \times 10^5 \frac{M_{BH}}{M_\odot} \text{cm}$. In comparison, the sun has a radius of $r_g \sim 7 \times 10^{10} \text{cm}$, or, roughly two-tenths of a million Schwarzschild radii.

2. *Time scale of variabilities: $t_g = r_g/c$.* This would be the shortest time scale of variation of quantities close to the black hole horizon. $t_v \sim 3 \times 10^{-5} \frac{M}{M_\odot} \text{s}$.

3. *Specific angular momentum: $l_g = r_g c$.* Matter with this angular momentum has a centrifugal force comparable to the gravitational force. $l_g \sim 9 \times 10^{15} \text{ cm sec}^{-1}$.

4. *Accretion Rate*: Eddington rate is $\dot{M}_{Ed} = 1.44 \times 10^{17} \frac{M_{BH}}{M_{\odot}} \text{gm sec}^{-1}$. This rate is determined by equating inward gravitational force on protons and the outward radiative force on electrons (e.g. [1]). \dot{M}_{Ed} is an upper limit of accretion rate, and is strictly valid for spherical flow on Newtonian stars and when the Thomson scattering is dominant. Critical rate is $\dot{M}_{Crit} = \dot{M}_{Ed}/\eta$, where, η denotes the efficiency of energy extraction from infalling matter. $\eta \sim 0.06$ for Schwarzschild black holes and $\eta \sim 0.4$ for extreme Kerr black holes.

5. *Luminosity*: Eddington luminosity is $L_{Ed} = \dot{M}_{Ed}c^2 = 1.3 \times 10^{38} \frac{M_{BH}}{M_{\odot}} \text{ergs sec}^{-1}$. The critical luminosity is L_{Ed}/η .

6. *Density of gas*: $\rho_g = \frac{\dot{M}_{Ed}t_g}{r_g^3} = 5.3 \times 10^{-5} \left(\frac{M_{BH}}{M_{\odot}}\right)^{-2} \text{gm cm}^3$.

7. *Virial Temperature*: $T_{virial} = \frac{1}{k} \frac{GM_{BH}m_p}{r_g} = 5.2 \times 10^{12} \text{K}$.

8. *Black Body Temperature*: $T_{BB} = \left(\frac{L_{Ed}}{\sigma r_g^2}\right)^{1/4} = 7.1 \times 10^7 \left(\frac{M_{BH}}{M_{\odot}}\right)^{-1/4} \text{K}$.

indent 9. *Magnetic fields*: Field strength is estimated from the assumption of equipartition: $B_E = (2\pi c^4 m_p / \sigma_T GM_{BH})^{1/2} \approx 3 \times 10^8 \frac{M_{BH}}{M_{\odot}} \text{G}$.

2.1 Effective Potential of Photons and Their Trajectories Around a Black Hole

Photons orbit in null geodesics governed by the metric of the spacetime. In Schwarzschild spacetime, the effective potential of photons is obtained from the null geodesic equation (GM_{BH}/c^2 is the length unit):

$$\left(\frac{dr}{d\lambda}\right)^2 = E^2 - \frac{l^2}{r^2}\left(1 - \frac{2}{r}\right) \quad (1a)$$

This can be rewritten as

$$\frac{1}{b^2} - \frac{1}{r^2}\left(1 - \frac{2}{r}\right) = \frac{1}{b^2} - V_{phot} = \left(\frac{dr}{d\lambda}\right)^2 \quad (1b)$$

The nature of the potential V_{phot} is shown in Fig. 1a. This shows that the photons with an impact parameter $b = l/E < 3\sqrt{3}$ would be swallowed by the hole. Here, $l = u_{\phi}$ is the specific angular momentum and $E = -u_t$ is the specific energy of a photon. If $b \gtrsim 3\sqrt{3}$, photon would escape. It would be interesting to know about the trajectories of photon around a black hole in

order to understand why it is difficult to detect it. The equation obeyed by photons around a Schwarzschild black hole is the null geodesic equation:

$$\left(\frac{du}{d\phi}\right)^2 = 2u^3 - u^2 + \frac{1}{D^2} \quad (2)$$

where, $u = 1/r$, $D = L/E$, $l = u\phi$.

Fig. 1b shows a collection of photon trajectories at different distances from a black hole. Shaded cone (‘absorption cone’) drawn at each radius indicates the directions in which photons are swallowed by the black hole. Photons emitted from the rest of the region (‘emission cone’) can escape to a large distance. Half angle ψ of the cones are given by $\psi = \sin^{-1} 3\sqrt{3}/[r\sqrt{(1-2/r)}]$. For instance, only half of the photons emitted isotropically from a point source at $r = 1.5r_g = 3GM_{BH}/c^2$ would escape to a large distance. This has a significant implications in spectral properties of black holes as will be discussed in Section 4. All the photons emitted from $r = r_g$ (dotted circle) are absorbed by the black hole. Hawking radiation emitted from immediate vicinity of a black hole horizon can come out due to quantum effects, but they will not be discussed here.

2.2 Effective Potential of Particles Around a Black Hole

Another interesting property of black holes which is often useful to identify them is the nature of the effective potential of a particle with a test mass. The effective potential of the particle is:

$$V_{eff} = \left[\left(1 + \frac{l^2}{r^2}\right)\left(1 - \frac{2GM_{BH}}{r}\right)\right]^{1/2}. \quad (3)$$

The potential starts developing a minimum when $l \gtrsim 2\sqrt{3}$. For $l < 2\sqrt{3}GM_{BH}/c$ the potential poses no obstruction to incoming matter, and matter can fall on to a black hole as easily as a spherical flow devoid of angular momentum. This is in sharp contrast with what is seen in a Newtonian geometry. Here, the effective potential is:

$$V_{eff,N} = 1 - \frac{GM_{BH}}{r} + \frac{l^2}{2r^2}. \quad (4)$$

which presents an infinitely high barrier to the flow with even an insignificant angular momentum. Fig. 2 shows the potential barrier both around a Schwarzschild black hole (solid curve) as well as around a Newtonian star (dashed) as a function of the radial distance (measured in units of GM_{BH}/c^2). The solid curves are drawn for (from bottom curve to the top curve) $l = 0, 2, 3, l_{ms} = 2\sqrt{3}, l_{mb} = 4$ & 5 respectively and the dashed curve is drawn for $l = 2$ (angular momenta are measured in units of GM_{BH}/c). l_{ms} is called the marginally stable angular momentum, since the closed orbits are impossible below this l . At $r = r_{ms} = 3r_g = 6GM_{BH}c^2$, $V_{eff}(l = l_{ms})$ has a point of inflection, and is called the marginally stable orbit. This closed orbit is the last stable orbit nearest to the black hole. For $r < r_{ms}$ matter cannot stay in a stable orbit and must dive into a black hole even with a slighted perturbation. This is an important ingredient in constructing accretion disk models as the inner sonic point where the flow becomes supersonic is close to this radius.

For $l_{mb} = 4GM_{BH}/c$, $V_{eff} = 1$ at $r_{mb} = 2r_g = 4GM_{BH}/c^2$. In this case, the orbit is marginally bound and the closest such orbit is located at r_{mb} . For $l \gtrsim l_{mb}$, $V_{eff} > 0$ in some region, and the matter will be bounced back to large distance. There is no bound orbit in region $r < r_{mb}$.

2.3 Fundamental Properties of Black Hole Accretion

Study of modern accretion processes on stars and compact objects began with the revolutionary work on spherical flows onto ordinary stars by Bondi [2], although the ‘black hole’ phrase was not known (at least in the context of Astrophysical object) at the time of that publication. Bondi solution was obtained in Newtonian geometry for pointlike mass. The general conclusion was that the subsonic (i.e., radial Mach number $M = v/a_s < 1$, where v is the radial velocity and a_s is the adiabatic sound speed of the infalling matter) flow with specific energy $\mathcal{E} \sim na_\infty^2 \geq 0$ (where n is the polytropic index of the flow, and a_∞ is the adiabatic sound speed at a large distance) which begins at rest at infinity would pass through a sonic point ($M = 1$) and remains supersonic $M > 1$ till the star surface where it stops and becomes subsonic. In this way, the boundary layer could be studied as a part of the inflow itself [3]. Alternatively, matter may remain subsonic throughout (e.g., [4]). For a black hole accretion, the flow passes through the horizon with the velocity of light, and therefore it must be supersonic on the horizon. These conclusions

are valid for rotating flows as well as for flows around rotating black holes [5]. For a recent review on spherical flows see, [4-6], and references therein.

With the Bondi solution in hand, the excessive luminosities of quasars and active galaxies in the sixties and seventies were readily conjectured to be due to gravitational energy release of matter accreting on black holes. However, it became apparent very soon that rapidly inflowing spherical matter is of very low density and advects virtually all the energy (save a small loss due to bremsstrahlung) through the black hole horizon. Magnetic dissipation could increase the efficiency of emission [7-8], but the assumptions which went in (for instance, equipartition of gas and magnetic fields) were not at all satisfactory. This is because the magnetic field and the gas are compressed at different rates: the pressure due to a radial field is compressed at $P_{mag} \propto r^{-4}$, while that due to adiabatic gas is compressed at $P_{gas} \propto r^{-5/2}$ (e.g., [9]). Equipartition achieved at any given radius is quickly off-balanced in another as the matter moves in. A serious problem is that locally excess energy of the magnetic field need not be dissipated within the disk itself, since the fields cannot be easily anchored in a stable disk as in a star [10]. Shakura & Sunyaev [11] and Novikov & Thorne [12] increased the efficiency of emission by assuming the flow to be rotating in Keplerian orbits just as in Saturn's ring. This basically rotating matter is of high density and the radiation emitted from this optically thick flow is roughly of black body type. The 'multicolour' black body emission (obtained by summing black body contributions from a large number of annuli on the disk) roughly agrees with the observed accretion disk spectra in binary systems as well as in active galaxies (see, e.g., [6] for references). One novel, though very simplifying, assumption made in this disk model is that one could quantify the unknown viscosity by using a so-called ' α ' parameter. The viscous stress $W_{r\phi}$ is simply written as $-\alpha P$, where P is the total pressure. This disk model (apart from a few corrections here and there) still remains the so-called 'standard model' after twenty five years of its introduction to the community.

This Keplerian description of purely rotating disk, is probably a bit too simplistic. Eardley & Lightman [13] solved the two temperature problem and pointed out that the Keplerian disk is viscously and thermally unstable if the viscosity parameter α is a constant throughout the disk. Even two decades ago, observed spectra of the black hole candidates, such as Cyg X-1 [14] indicated that the spectrum consists of two distinct components. The soft X-ray bump in these spectra could be explained by multicolour black body emis-

sion from a Keplerian disk. The power-law component of the spectra was explained by Comptonization of softer photons by hot electrons from ‘Compton clouds’, or, magnetic corona [15-19]. The softer photons originate from a Keplerian disk, and the origin of the Compton cloud including magnetic corona remained unspecified, until recently, when it was realized that the so-called Compton cloud is probably the inner part of the disk itself when the disk is described by advective flow [20-21]. The behaviour of the power-law component was complex: the energy spectral index α ($F_\nu \propto \nu^{-\alpha}$) apparently stays closer to 0.5–0.7 when the soft bump is very weak or non-existent (and remains almost constant even when the intensity of the soft bump changes by a factor of several), and closer to 1.5 when the soft bump is very strong. (Note that we are using the same customary notation α to denote the viscosity parameter as well as the energy spectral index. But this will not cause confusion.) In the first case, most of the power is emitted in the hard component and the black hole is said to be in the ‘hard state’. In the second case, most of the power is emitted in the soft component and the black hole is said to be in ‘soft state’ [20, 22-23 and references therein]. The energies of the so-called ‘soft’ and ‘hard’ radiations depend on the mass of the black hole. For a stellar black hole (typically resulting from a supernova explosion) of mass $10M_\odot$, the soft radiation bump would be in $\sim 1 - 3\text{keV}$, while for a super-massive black hole (typically resulting from protogalactic collapse at the center of galaxies) of mass $10^{8-9}M_\odot$, the soft radiation bump would be in the extreme ultraviolet (EUV) to ultraviolet (UV) region. Hard radiations of 100keV or even up to an MeV are not uncommon in both types of black holes. Typical Compton spectra using Sunyaev-Titarchuk [15]) type analysis suggests that in the low state the electron temperature of the hot region is roughly 100 – 200keV for stellar mass black holes and around 40 – 60keV for super-massive black holes.

The nature of the emitted radiation is clearly very complex and no simple solution such as the Bondi flow or a Keplerian disk could explain it completely. In reality, of course, it is difficult to form either of these flows anyway. Since the incoming flow must have some angular momentum as it is coming from an orbiting companion (as in a binary system) or some orbiting stars (as in a galactic nucleus), the flow cannot be purely Bondi-like. Similarly, the inner boundary condition on the horizon (that the flow velocity be equal to the velocity of light) suggests that the flow must be supersonic, and hence sub-Keplerian at least close to the horizon [6, 24]. Again, unlike in a

Keplerian disk, where Keplerian distribution is guaranteed whatever viscosity is present, in a realistic flow (which includes advection by default), the angular momentum distribution is to be determined self-consistently from the transport equations. It may join a Keplerian disk at several tens to hundreds of Schwarzschild radii away depending on the specific energy, angular momentum and viscosity. Thus a realistic flow *must* be an intermediate solution between the Bondi flow and a Keplerian disk. If the specific energy is positive, the advective flow would have the ability to pass through two saddle type sonic points through shocks (but need not have shocks always, especially when the Rankine-Hugoniot conditions are not satisfied), but if the specific energy is negative, it may pass through only one sonic point and join with a cold Keplerian disk farther away. These conclusions are valid for *any* accretion rate or viscosity. For higher accretion rates, the advective flow should cool down due to Comptonization, but then the energy would come down to negative. Sustained magnetic heating, could keep the energy to be positive and therefore flow can remain advective. Far away from the black hole, the flow may be cold and Keplerian (may even be sub-Keplerian if matter is accreted from a large number of stars), but close to the black hole, the flow must be sub-Keplerian. Apart from this deviation of the angular momentum distribution, the geometrical shape and internal dynamics of matter are also very much changed from a standard model. The presence of some angular momentum causes the centrifugal barrier supported geometrically thick region to be formed around a black hole whose property is similar to that of a boundary layer. This we call CENBOL (CENTrifugally supported BOundary Layer). The evolution of the accretion disk model is schematically shown in Fig. 3(a-c): In 3(a) the Bondi flow; in 3(b), the Keplerian disk and in 3(c), the generalized advective disk are shown. The figure in 3(c) is based on combination of advective disk solutions in different regime. Beside each model, a typical spectrum is also schematically shown in $\nu \log(F_\nu)$ vs. $\log(\nu)$ scale. In (a), the spectrum is hard, mostly due to bremsstrahlung; in (b), the spectrum is soft and multicolour blackbody type, and in (c), it is the combination of the soft X-ray and hard X-ray emitted from the disk. In 3(c), variation of the spectra relative accretion rates in the Keplerian and sub-Keplerian components (or, equivalently, viscosity variation in the disk) is shown where the transition from the hard to soft state is achieved.

In this context, it is to be noted that advective accretion flows are those which self-consistently include advection velocity as in Bondi flows at the

same time include rotation, viscosity, heating and cooling processes. For a black hole accretion, these are the same as viscous transonic flows (VTF) discussed in detail in Chakrabarti [5, 25]. Special cases of VTFs are the so called slim disks for optically thick flow [26] and Advection Dominated Flows for optically thin flow [27]. However, global solutions of these special cases were not found to be satisfactory [5]. Thus, we use the more general advective disk solution. For a neutron star accretion, the flow need not be transonic (e.g., could be subsonic everywhere) and the advective disks include that possibility as well.

There are several models in the literature which were brought in to explain different observational features from time to time. These are far from self-consistent and serve only special purpose for which they were invoked. Foundation of the advective disk solution discussed here, on the contrary, is on the most general set of equations from which all other models emerge as special cases. It is therefore no surprise that this solution seems to have the ‘right features in the right regime’. The Bondi flow and the Keplerian disks are both extreme cases: one does not have rotation and the other does not have advection properly included. The first one is basically energy conserving (roughly valid for low accretion rate) spherical advective flow and the second one is highly dissipative (roughly valid for viscous, high accretion rate) disklike flow. Attempts to fill the gap, i.e., to find intermediate structures were made since early eighties. Paczyński and his collaborators advanced models in two different directions: (1) Thick accretion disks [28] and references therein): where the flow is still rotation dominated, but non-Keplerian. The radiation pressure is high enough to hold matter vertically, preventing it from collapsing. This thick disk model was clearly valid for high accretion rate and the radiation pressure in the funnel was assumed to push matter vertically to form outflows and jets. Rees et al. [29] pointed out that the low accretion rate flow can support vertical structure due to strong ion pressure while most of the energy is advected. These models were not globally complete as the disk is generally non-accreting. (2) Transonic flows [30-31]: Here the radial motion is also included but global solutions were not explored. Preliminary non-dissipative solutions indicated [32] that unlike Bondi flow, there are two saddle type sonic points in an advective flow. Abramowicz & Zurek [33] further concluded that the same matter could go through the outer (Bondi) or inner (disklike) sonic points, although it is now known that they have different entropies and should be counted as by

two different flows unless connected by standing shocks (see, [5] for details.). Matsumoto et al. [34] tried to mend the inner edge of the Keplerian disk (although the sonic point was chosen to be nodal) while Abramowicz et al. [26], in the so-called slim disk tried to find global solutions of the transonic flow in the high accretion rate limit without success (although local solutions were seen to be stable due to advection). The transonic solution of Fukue [35] had a standing shock wave very similar to those in winds by Ferrari et al. [36]. Chakrabarti [3, 5, 25] found all possible topologies of advective disk solutions in viscous and non-viscous flows, with and without magnetic fields. The recently re-discovered ion tori [29] (dubbed as advection dominated flow) by [27, 37] is as ad hoc as its predecessor since it is assumed to behave something like ‘corona without a disk’. This corona comes about by inexplicable evaporation method of the underlying Keplerian disk at a low accretion rate. The spherical distribution of matter that comes about (see Fig. 1 of Narayan [38]) even when angular momentum is included is equally inexplicable. (This controversial solution or its consequences are clearly irrelevant in black hole astrophysics and will not be discussed in this review any farther.) The post-shock and/or the CENBOL regions of advective disk solutions [3, 5, 25] resemble those of thick disks (but accreting!). High accretion rate solutions of advective disk are the globally correct solutions of ‘slim disks’ (unlike Abramowicz et al., [26] model, these advective flows have angular momentum correctly approaching a Keplerian disk) and low accretion rate advective disks are the correct ‘advection dominated flows’ (unlike Narayan & Yi, [27, 37, 38] model, these flows naturally deviate from a Keplerian disk specially for low viscosity and positive specific energy and NOT for high viscosity, and no evaporation is required). Recently, some groups are attempting to try to reproduce advective disk solutions in their respective regimes [39-40]. The success has been limited because of less general approach of solving the eigenvalue problem that the equations posit. In their approach the flow is ‘let loose’ from a Keplerian disk at an arbitrary distance with an arbitrary initial radial and angular velocity components and only one sonic point is assumed (thus by construction this method cannot find shocks, for instance, even when the specific energy is positive). In the advective disk approach [3, 5, 25] the flow is also allowed to have ‘discontinuous’ (shock) solutions which joins two branches passing through two sonic points. When such joining is not possible, the inflow shows non-stationary behaviour, unless only one sonic point is present to begin with. With viscosity variation,

the net accretion flow is Keplerian disklike in some region, and advective in some other region. Today, the need for having the admixture of Keplerian and sub-Keplerian components (as first quantitatively pointed out by [20]) in the accretion flows is clearly recognized in most of the observations.

An accretion disk must fall in and advect. It was on this philosophy Bondi flow was studied originally. In the intervening period, specially, in the seventies and early eighties, rotating Keplerian disk took over while inclusion of advection was considered to be a ‘new model’! The question of whether an advective disk can explain observations is outright irrelevant because this disk represents the only self-consistent solution of the governing equations which are derived from fundamental laws of nature (such as conservation of energy and momentum). The same solution produces boundary layer of black holes (specifically for hot flows) and neutron stars. The importance of CENBOL was not appreciated originally, but now they are indispensable in most explanations, given that they obviate the need to construct ad hoc ‘Compton Clouds’ (e.g., [41-42], and references therein). The future of the black hole astrophysics is most certainly the correct understanding of the CENBOL region of the flow.

In order to establish the general behaviour of matter described above, we now present all the possible solutions of non-self-gravitating test flow around a Kerr black hole. We use t , r , θ and z as the coordinates. We choose the geometric units where $G = M_{BH} = c = 1$ (G is the gravitational constant, M_{BH} is the mass of a black hole and c is the velocity of light). We also consider $|\theta - \pi/2| \ll 1$ for a thin flow on the equatorial plane in vertical equilibrium. We consider a perfect fluid with the stress-energy tensor,

$$T_{\mu\nu} = \rho u_\mu u_\nu + P(g_{\mu\nu} + u_\mu u_\nu) \quad (5)$$

where, P is the pressure and $\rho = \rho_0(1 + \pi)$ is the mass density, π being the internal energy. We ignore the self-gravity of the flow as well as the contribution due to viscous dissipation. We assume the vacuum metric around a Kerr black hole to be of the form [12],

$$ds^2 = g_{\mu\nu} dx^\mu dx^\nu = -\frac{r^2 \Delta}{A} dt^2 + \frac{A}{r^2} (d\phi - \omega dt)^2 + \frac{r^2}{\Delta} dr^2 + dz^2 \quad (6)$$

Where,

$$A = r^4 + r^2 a^2 + 2ra^2 \quad (7a)$$

$$\Delta = r^2 - 2r + a^2 \quad (7b)$$

$$\omega = \frac{2ar}{A}. \quad (7c)$$

Here, $g_{\mu\nu}$ is the metric coefficient and u_μ is the four velocity components:

$$u_t = - \left[\frac{\Delta}{(1 - V^2)(1 - \Omega l)(g_{\phi\phi} + l g_{t\phi})} \right]^{1/2} \quad (8a)$$

and

$$u_\phi = -l u_t \quad (8b)$$

where, the angular velocity is

$$\Omega = \frac{u^\phi}{u^t} = - \frac{g_{t\phi} + l g_{tt}}{g_{\phi\phi} + l g_{t\phi}} \quad (9)$$

and $l = -u_\phi/u_t$ is the specific angular momentum. The radial velocity V in the rotating frame is (see, [25] p. 137)

$$V = \frac{v}{(1 - \Omega l)^{1/2}} \quad (10)$$

where,

$$v = \left(-\frac{u_r u^r}{u_t u^t} \right)^{1/2}. \quad (11)$$

It is trivial to check that V above is unity on the horizon independent of the initial condition.

Since even for the extreme equation of state $P = \frac{1}{3}\rho_0 c^2$, (p is the isotropic matter pressure and ρ is the rest mass density), the speed of sound is $a_s = \frac{1}{\sqrt{3}}$, the Mach number of the flow is $M = v/a_s = \sqrt{3} > 1$, any physical flow must be *supersonic* on the horizon. This inner boundary condition has a profound effect on the structure of the accretion disk around a black hole as we will see here.

In the present review, we shall concentrate on the time independent solutions of the underlying hydrodynamic equations. The equation for the balance of the radial momentum is obtained from $T_{;\alpha}^{\mu\alpha} = 0$:

$$\vartheta \frac{d\vartheta}{dr} + \frac{1}{r\Delta} \left[a^2 - r + \frac{A\Gamma^2 B}{r^3} \right] \vartheta^2 + \frac{A\Gamma^2}{r^6} B + \left(\frac{\Delta}{r^2} + \vartheta^2 \right) \frac{1}{p + \rho} \frac{dP}{dr} = 0 \quad (12)$$

where,

$$\Gamma^2 = [1 - \frac{A^2}{\Delta r^4}(\Omega - \omega)]^{-1}, \quad (13)$$

$$B = (\Omega a - 1)^2 - \Omega^2 r^3, \quad (14)$$

and

$$\vartheta = u^r. \quad (15)$$

Here and hereafter a comma is used to denote an ordinary derivative and a semi-colon is used to denote a covariant derivative. The baryon number conservation equation (continuity equation) is obtained from $(\rho_0 u^\mu)_{;\mu} = 0$ which is,

$$\dot{M} = 2\pi r \vartheta \Sigma = 2\pi r \vartheta \rho_0 H_0 \quad (16)$$

where,

$$H_0 = \left(\frac{P}{\rho_0}\right)^{1/2} \frac{r^{3/2}}{\Gamma} \left[\frac{(r^2 + a^2)^2 - \Delta a^2}{(r^2 + a^2)^2 + 2\Delta a^2} \right]^{1/2} \quad (17)$$

is the height of the disk in vertical equilibrium [12]. The equation of the conservation of angular momentum is obtained from $(\delta^{\mu\phi} T'_{\mu\alpha})_{;\alpha} = 0$, and one obtains,

$$\rho_0 u^\mu (h u_\phi)_{;\mu} = (\eta \sigma_\phi^\gamma)_{;\gamma} \quad (18)$$

where,

$$\eta = \nu \rho_0 \quad (19)$$

is the coefficient of dynamical viscosity and ν is the coefficient of kinematic viscosity. The stress-energy tensor $T'_{\mu\nu}$ contains the term due to viscous dissipation (e.g., [43]). When the rotation is dominant ($\vartheta < u^\phi$), the relevant shear tensor component σ_ϕ^r is given by [44],

$$\sigma_\phi^r = -\frac{A^{3/2} \Gamma^3 \Omega_{,r} \Delta^{1/2}}{2r^5} \quad (20)$$

so that the angular momentum equation takes the form [24],

$$\mathcal{L} - \mathcal{L}_+ = -\frac{1}{\vartheta r^5} \frac{d\Omega}{dr} \nu A^{3/2} \Gamma^3 \Delta^{1/2}. \quad (21)$$

Here, we have corrected the angular momentum transport equation of Novikov & Thorne [12] as derived in [24]. In this equation on the left hand side,

the fluid angular momentum $\mathcal{L} = hu_\phi$ [24] rather than particle angular momentum u_ϕ [12] has been used. For an inviscid flow, $\eta = 0$ one recovers $\mathcal{L} = \text{constant}$ as it should be. Similarly, the radial velocity term is included (eq. 12) and angular momentum is allowed to be non-Keplerian (eq. 21). \mathcal{L}_+ is the angular momentum on the horizon since the *rotational* shear (as defined by eq. 20) vanishes there. In presence of significant radial velocity, the shear in eq. (20) is to be replaced by its full expression, $\sigma^{\mu\nu} = (u_{;\beta}^\mu P^{\beta\nu} + u_{;\beta}^\nu P^{\beta\mu})/2 - \Theta P^{\mu\nu}/3$ where $P^{\mu\nu} = g^{\mu\nu} + u^\mu u^\nu$ is the projection tensor and $\Theta = u^\mu_{;\mu}$ is the expansion [1].

Entropy generation equation is obtained from the first law of thermodynamics along with the baryon conservation equation $(S^\mu)_{;\mu} = [2\eta\sigma_{\mu\nu}\sigma^{\mu\nu}]/T - Q^-$:

$$\vartheta\Sigma\left(\frac{dh}{dr} - \frac{1}{\rho_0}\frac{dp}{dr}\right) = Q^+ - Q^- = 2\nu\Sigma\sigma_{\mu\nu}\sigma^{\mu\nu} - Q^- \quad (22)$$

where Q^+ and Q^- are the heat generation rate (by viscosity, exothermic nuclear energy generation, magnetic dissipation, etc.) and the heat loss rate (by radiative cooling, by endothermic reactions, etc.) respectively. h is the specific enthalpy: $h = (p + \rho)/\rho_0$. Here, the terms contributed by radiation have been ignored as well. Using rotational shear as given in eq. (20), the entropy equation takes the form,

$$\vartheta\Sigma\left(\frac{dh}{dr} - \frac{1}{\rho_0}\frac{dp}{dr}\right) = \frac{\nu\Sigma A^2\Gamma^4(\Omega_{,r})^2}{r^6} - Q^-. \quad (23)$$

Of course, for accuracy, one should use the full expression for σ_ϕ^r .

This set of equations are solved simultaneously keeping in mind that the shock waves may form in the flow, especially when the specific energy is positive. The following momentum balance condition [24],

$$W_-n^\nu + (W_- + \Sigma_{0-})(u_-^\mu n_\mu)u_-^\nu = W_+n^\nu + (W_+ + \Sigma_{0+})(u_+^\mu n_\mu)u_+^\nu \quad (24)$$

along with the conservation of energy and mass fluxes (together, these conditions are known as the Rankine-Hugoniot conditions) must be fulfilled at the stationary shock. Here, n_μ is the four normal vector component across the shock, and W and Σ are vertically integrated pressure and density on the shock surface. Here, the subscripts $-$ and $+$ denote the pre-shock and post-shock quantities respectively.

The equations presented above are applicable to optically thin as well as optically thick flows for any general heating and cooling processes. For a given viscosity prescription and the exact cooling processes (depending on the optical depth of the flow), it is usual to reduce the above set of equations in the form:

$$\frac{du}{dr} = \frac{N}{D} \quad (25)$$

where, N and D are the smooth functions of radial coordinate (unless there are non-linearities which prevent such a reduction. In that case sonic curve analysis is done, see, Castor, Abott & Klein [45] in Newtonian context and Flammang, [46] in general relativistic winds). The procedure of obtaining the complete solution is then similar to what is presented in obtaining the global solutions of viscous transonic flow using pseudo-Newtonian potential ([5, 25] and references therein). We shall present the complete set of solutions of these equations shortly. Before doing so, we prove two fundamental points about the advective flow.

2.3.1 Flow Must be Sub-Keplerian on the Horizon

We first rewrite B of equation (12) as

$$B = -(\Omega - \Omega_{K+})(\Omega - \Omega_{K-}) \quad (26)$$

where,

$$\Omega_{K\pm} = \pm \frac{1}{r^{3/2} \pm a} \quad (27)$$

are the Keplerian angular momenta for the co- (plus sign) and contra- (minus sign) rotating flows. From eqn. (12) one notes that since $u' < 0$ and $p' \sim 0$ on the horizon, one must have,

$$B > 0 \quad (28)$$

on the horizon, i.e., $\Omega < \Omega_{K+}$, or $l < l_{Kep}$. This can also be shown more generally context by computing a_s^2 at the sonic point and imposing the condition that $a_s^2 > 1$. It is seen that at the sonic point the flow must be sub-Keplerian. In the inviscid flow, this means that the sonic point should form only in sub-Keplerian region. In presence of viscosity, since angular momentum transport rate is almost zero close to the horizon and the distribution is almost flat (see, Fig. 6), the flow would maintain the sub-Keplerian nature between the inner sonic point and the horizon.

2.3.2 Rotating Flow Must Have a Centrifugal Barrier

An important ingredient of the state-of-the-art accretion flow is the centrifugal pressure supported denser region close to a black hole. Roughly speaking, the infall time scale being very short compared to the viscous (transport of angular momentum) time scale, the angular momentum l remains almost constant close to the black hole particularly for lower viscosity. As a result, the centrifugal force l^2/r^3 increases much faster compared to the gravity $\sim 1/r^2$ as the flow approaches the black hole. Matter starts piling up behind this centrifugal barrier and becomes denser, with opacity $\tau \sim \dot{m}$, where \dot{m} is the accretion rate in units of the Eddington rate. Eventually, of course, the gravity wins and the matter enters into the black hole supersonically. Since the effective potential turns over for any angular momentum, matter with any amount of angular momentum can be made to accrete on a black hole if it is ‘pushed’ hard enough. This is to be contrasted with the fact that an infinite force is required to push matter to the surface of a Newtonian point mass with even an insignificant angular momentum (Fig. 2). This is why a rotating flow has a saddle type sonic point close to a black hole, while the closest sonic point for a Newtonian rotating flow is of unphysical ‘center’ type. This will be demonstrated below.

At the centrifugal pressure supported barrier (CENBOL), matter slows down and its thermal energy increases. In some region of the parameter space this slowing down takes place rather abruptly at a standing shock. Most of the thermal energy of the flow could be extracted from this region through inverse Compton effect if soft photons are injected here from the Keplerian disk component. Whereas the boundary layer of a white dwarf is of thickness less than a percentage of its radius, the thickness of the boundary layer (CENBOL) of a black hole is several (typically, 10 – 20) times larger than its radius! If the neutron star is not compact enough (i.e., not within the inner sonic point of the flow), its boundary layer would also be of similar size. For compact neutron stars, the boundary layer could be very thin because the shock transition (x_{s1} , or r_{s1} in the notation of [3]) just outside the hard surface is allowed, unless the entire flow is subsonic. Absence of a centrifugal barrier in a Bondi flow causes the flow to be inefficient and one requires sufficient magnetic field to enhance the cooling efficiency [7, 8]. It is not to say that such enhancement should not take place, or, is not completely required in advective disks in explanation of spectra (especially at high energies when

synchrotron radiation plays a major role), but so far, the inclusion of the magnetic fields has not been done consistently. In a self-similar flow, one equipartition of gas and magnetic field is achieved, it is always maintained. But the flow is hardly self-similar, with sonic points, possible shocks, Keplerian flow boundaries etc. The major problem lies in deciding what fraction of the magnetic field could be used for heating electrons (to enter in the Q^+ term in eq. 22), given that most of the excess field may be expelled away in absence of adequate anchoring of the field on the disk [10].

CENBOL happens to have just the right set of properties: the efficiency of its emission is neither almost zero as in a Bondi flow, nor fixed and maximum as in a Keplerian disk. Its size and optical depth are determined by viscosity and accretion rates and therefore give rise to varieties of spectral properties as are observed. The present review primarily emphasizes ways to identify black holes and therefore, ways in which CENBOL manifests itself in various observational phenomena. We discuss extensively how the spectral properties, both steady and non-steady, soft state and hard state, may be dependent on the properties of the CENBOL. We also show that as spin-offs, it may help supplying matter to the cosmic radio jets, explain metallicity of the galaxies and a host of other effects.

2.4 All Possible Ways to Dive into a Black Hole

We now present all possible ways matter can enter into a black hole. In obtaining a global solution one supplies the conserved quantities at the inner or the outer (e.g., Keplerian or sub-Keplerian flows injected at the outer region) boundary, depending upon whether one is interested in the wind solution or the accretion solution. For a given angular momentum l , the remaining unknowns are $V(r)$ and $a_s(r)$. But one requires only one extra boundary condition, e.g., \mathcal{E} , since two sonic point conditions (eqs. 31a and 31b) introduce only one extra unknown, namely, r_c . Thus, the supply of the initial specific energy \mathcal{E} and the specific angular momentum l are sufficient for a complete solution from the horizon to infinity. For a viscous flow, one clearly has to supply the distribution of viscosity $\eta(r)$ (e.g., ion or magnetic viscosity) itself. Simple viscosity prescription [11] may not be very useful since that stress $-\alpha P$ is always negative, while in a general relativistic flow stress can change sign [24, 44]. the total pressure $P + \rho V^2$ (i.e., including ram pressure) is more appropriate than just P , especially when advection is

significant [47]. Note that by definition, $\Omega = \omega$ on the horizon and thus the flow co-rotates with the black hole. Instead of specifying various quantities at the flow boundary, one can alternatively specify the location of a critical point along with the energy or the angular momentum [25].

In much of the parameter space, the flow is expected to be smooth as in a Bondi flow. If the angular momentum is significant, matter can pile up behind the centrifugal barrier close to the black hole and form a standing shock wave where several quantities are actually discontinuous. At the shock, apart from the continuity of energy and mass flux, the relativistic momentum balance condition (eq. 24) must be satisfied. Using Newtonian definition of the vertical integration (since thin flows are being dealt with here) as in [3] and the definition of entropy accretion rate $\dot{\mathcal{M}}$, one easily finds that at the shock, the following quantity:

$$\Pi = \frac{\left[\frac{a_s^2}{1-na_s^2} \right]^{n+3/2} \left(\frac{2}{3\Gamma-1} + \frac{V^2}{a_s^2(1-V^2)} \right)}{\dot{\mathcal{M}}} \quad (29)$$

should be continuous. At the shock, entropy is generated (turbulent or other viscosities operating at the shock) which is then advected through the inner sonic point.

In this context, it is important to point out that eq. (29) is valid only for Rankine-Hugoniot shocks where the energy flux is continuous. In an astrophysical flow which is open to surroundings, this need not be so and both energy and entropy could be lost to the surroundings. It has been estimated that one can release a burst of photons at the shock which could contain as high as a couple of percents of the rest mass energy [48, 49]. This is important. Potentially releasable energy even for an optically thin flow may not be released at all and may be completely advected towards the black hole.

The considerations mentioned above are valid for object whose external spacetime is similar to that of a Kerr black hole. On a neutron star surface, however, matter has to stop and corotate with the surface velocity. The inner boundary condition is therefore sub-sonic. On a black hole, the flow must enter through the horizon with the velocity of light, and therefore must be supersonic. The supersonic flow becomes subsonic at the shock and again becomes supersonic before entering through the horizon. Clearly, the flow has to become supersonic, before forming the shock as well, and therefore

pass through another sonic point at a larger distance away from the black hole. Thus, as a whole, the flow may deviate from a hot Keplerian disk and (a) enter through the inner sonic point only, or, (b) enter through the outer sonic point only, or, (c) pass through the outer sonic point, then a shock, and finally through an inner sonic point if the shock conditions are satisfied. If the angular momentum is too small, then the flow has only one sonic point and shocks cannot be formed as in a Bondi flow.

In Fig. 4, the *entire* parameter space is classified according to the type of inviscid solutions that is prevalent [24]. The Kerr parameter $a = 0.5$. (For classification of flows in pseudo-Newtonian geometry, see, [3, 21, 25]). The adiabatic index $\gamma = 4/3$ has been chosen. In the central box, the parameter space spanned by (l, \mathcal{E}) is divided into nine regions marked by $N, O, NSA, SA, SW, NSW, I, O^*, I^*$. The horizontal line at $\mathcal{E} = 1$ corresponds to the rest mass of the flow. Surrounding this parameter space, we plot various solutions (Mach number $M = v_r/a_s$ vs. logarithmic radial distance where v_r is the radial velocity and a_s is the sound speed) marked with the same notations (except N). Each of these solution topologies has been drawn using flow parameters from the respective region of the central box. The accretion solutions have inward pointing arrows and the wind solutions have outward pointing arrows. The crossing points are ‘X’ type or saddle type sonic points and the contours of circular topology are around ‘O’ type sonic points. If there are two ‘X’ type sonic points, the inner one is called the inner sonic point and the outer one is called the outer sonic point. The solutions from the region ‘O’ has only the outer sonic point. The solutions from the regions NSA and SA have two ‘X’ type sonic points with the entropy density S_o at the outer sonic point *less* than the entropy density S_i at the inner sonic point. However, flows from SA pass through a standing non-dissipative shock since the Rankine-Hugoniot condition is satisfied. The entropy generated at the shock $S_i - S_o$ is advected towards the black hole to enable the flow to pass through the inner sonic point. Rankine-Hugoniot condition is not satisfied for flows from the region NSA . Numerical simulations indicate [50] that the flow from this region is very unstable and exhibit periodic changes in emission properties as the flow constantly tries to form the shock wave, but fails to do so. Thus, it is possible that the solutions are inherently time-dependent (just as a simple harmonic oscillator) in this region. The solutions from the region SW and NSW are very similar to those from SA and NSA . However, $S_o \geq S_i$ in these cases. Shocks can form only in winds from the region SW .

The shock condition is not satisfied in winds from the region NSW . This may make the NSW winds unstable as well, but the accretion through the inner sonic point is stable. A flow from the region I has the inner sonic point and thus can form shocks (which require the presence of two saddle type sonic points) only if the inflow is already supersonic due to some other physical processes. Each solution from regions I^* and O^* has two sonic points (one ‘X’ and one ‘O’) and neither of them produces a complete and global solution. The region I^* has an inner sonic point but the solution does not extend subsonically to a large distance. The region O^* has an outer sonic point, but the solution does not extend supersonically to the horizon! When a significant viscosity is added, the closed topology of I^* opens up and then the flow joins with a cool Keplerian disk [5, 25] which has $\mathcal{E} < 1$. These special solutions of viscous transonic flows should not have shock waves. However, hot flows deviating from a Keplerian disk or sub-Keplerian companion winds can have $\mathcal{E} > 1$ or, cool flows can be subsequently energized by magnetic flares (for instance). These could have standing shock waves as discussed above. Energetically, the flow should have $\mathcal{E} > 0$ as in a Bondi flow, to pass through the outer sonic point, which is a pre-requisite to form standing shocks.

In [3] and [25], it was found that shock conditions were satisfied at four locations: r_{s1} , r_{s2} , r_{s3} and r_{s4} , though r_{s1} and r_{s4} were found to be not useful for accretion on black holes. Out of r_{s2} and r_{s3} , it was shown that r_{s3} is stable for accretion flow and r_{s2} is stable for winds ([51] also see, [49, 52-54]). So we have plotted only r_{s3} here in SA and r_{s2} in SW solutions. Here, o and i are the outer and inner sonic points respectively. In the solution from SA (upper left box in Fig. 4), we chose $a = 0.5$, $l = 3$, $\mathcal{E} = 1.003$. For these parameters, the eigenvalue of the critical entropy accretion rates at the two saddle type sonic points are $\dot{\mathcal{M}}_i = 2.74 \times 10^{-05}$ and $\dot{\mathcal{M}}_o = 1.491 \times 10^{-05}$ respectively. Here, $\dot{\mathcal{M}}_o < \dot{\mathcal{M}}_i$, hence the flow through the outer sonic point joins the horizon with infinity (single arrowed curve). The flow forms a shock and jump onto the branch which passes through i as shown by double arrows. The stable shock (shown by a vertical dashed line) is located at $a_3 = r_{s3} = 32.29$ (in notation of [3]). Only this jump, namely, a generation of entropy of amount $\dot{\mathcal{M}}_i - \dot{\mathcal{M}}_o$ is allowed in order that the transonicity of the post-shock flow is guaranteed. The entropy generated at the shock is advected through the inner sonic point. The optically thin flow is inefficiently cooled, which keeps the energy of the flow constant. This makes the flow much hotter than a

Keplerian disk. (This is typical of advective disks. See, [3], [25], [55].) In *SW* solution, we chose $a = 0.5$, $l = 3$, $\mathcal{E} = 1.007$. For these parameters, the eigenvalue of the critical entropy accretion rates at the two saddle type sonic points are $\dot{\mathcal{M}}_i = 3.12 \times 10^{-05}$ and $\dot{\mathcal{M}}_o = 5.001 \times 10^{-05}$ respectively. Here, $\dot{\mathcal{M}}_i < \dot{\mathcal{M}}_o$, hence the flow through the inner sonic point i joins the horizon with infinity (single arrowed curve). The accretion flow branch can no longer form a shock. But a wind, first passing through i can, as shown in double arrows. The stable shock (shown by a vertical dashed line) is located at $w_2 = r_{s2} = 6.89$ in this case. Only this jump, namely, a generation of entropy of amount $\dot{\mathcal{M}}_o - \dot{\mathcal{M}}_i$ is allowed at the shock in order that it can escape to infinity through the outer sonic point O . This consideration, along with the continuity of Π (Eq. 19) allows one to locate stationary shock waves in a flow. Note that though the flow has a shock-free solution (passing through o for accretion in *SA* solution and through i for winds in *SW* solution in Fig. 4), the flow would choose to pass through a shock because the latter solution is of higher entropy. This fact has been verified through numerical simulations of accretion and wind flows [51, 56]. It is to be noted that the angular momenta associated with solutions which include shocks are not arbitrarily large. Rather, they are typically less than the marginally stable value l_{ms} as indicated in Fig. 4.

Global solutions which contain shock waves are not isolated solutions, but are present for a large range of energy and angular momentum. In Fig. 5, the variation of shock locations as a function of specific energy \mathcal{E} is shown. Each set of curves, drawn for various specific angular momentum (marked on the set), consists of four segments: two for accretion ($a_2 = r_{s2}$ and $a_3 = r_{s3}$) and two for winds ($w_2 = r_{s2}$ and $w_3 = r_{s3}$). As discussed above, a_2 and w_3 (dotted curves) are unstable while a_3 and w_2 (solid curves) are stable. Kerr parameter $a = 0.5$ is chosen. This example shows that stable shocks can form for a very wide class of flows. For corotating flows, the marginally stable and marginally bound angular momenta are $l_{ms} = 2.9029$ and $l_{mb} = 3.4142$ respectively. Thus the shocks form for angular momentum around these values. Since centrifugal barrier becomes stronger with angular momentum, shocks are located at larger radii for higher angular momenta. Another important point to note is that the shock location increases when the specific energy is increased. In a quasi-spherical flow, with the same input radial velocity and angular momentum, the potential energy decreases with height (since the gravity becomes weaker), thereby increasing the specific

energy and therefore shocks bend backward with height. General statements made for the shocks are valid for the CENBOL as well, where shock itself is not formed, but the density and velocity variation follow the same general pattern.

The solution branch which is supersonic close to the axis is valid for black holes while the solution branches subsonic close to the axis are valid for neutron stars. This is discussed in details in [3] and more recently in [4]. The solution entering through the horizon is unique, since it must pass through the sonic point. This is physically appealing since the properties of the horizon are independent of any physical parameters such as temperature and pressure of the gas etc. The solution touching a neutron star surface is not unique in the same token since any number of subsonic branches from infinity can come close to the axis (either through shocks or without shocks). Of course, ultimately, the one which matches with the surface properties of the star will be selected. In a black hole accretion, such choices are simply not present.

2.5 Solution topologies of Viscous Flow

When viscosity is present, three (instead of two) flow parameters govern the topology of the flow: the α parameter [11] or, its modified value α_{Π} in presence of advection [47], which determines the viscosity, the location of the inner sonic point x_{in} through which matter must pass through, and the specific angular momentum l_{in} of the matter at the horizon (or, alternatively, that at r_{in}). It so happens that these parameters are sufficient to completely determine the solution. Unfortunately, majority of the works in black hole astrophysics has been done, not by using full fledged general relativity, but using pseudo-Newtonian geometry. Paczyński & Wiita [28] pointed out that outside the Schwarzschild black hole, the spacetime may be described using Newtonian equations, but changing the $-GM_{BH}/r$ potential to $-GM_{BH}/(r - 2GM_{BH}/c^2)$ potential. There are small deviations when fully general relativistic and Pseudo-Newtonian calculations are compared, but for all practical purposes the deviations are tolerable. The *nature* of classification of the parameter space as well as the *nature* of the variation of shock locations as described above are valid for for all Kerr parameters and is independent of the flow model that is employed as long as $\gamma < 1.5$ [5, 25] though details vary from model to model [note that in [21], ‘ $\gamma < 1.5$ ’

was misprinted as ‘ $\gamma > 1.5$ ’]. For $\gamma > 1.5$, two sonic points are not present in an adiabatic flow (but may be present if external heating is included for instance) and therefore the shocks cannot form, but the centrifugal barrier would still exist as described in [5].

Typical hydrodynamic equations which govern vertically averaged advective flows in the pseudo-Newtonian geometry are as follows [5],

(a) The radial momentum equation:

$$v \frac{dv}{dx} + \frac{1}{\rho} \frac{dp}{dx} + \frac{\lambda_{Kep}^2 - \lambda^2}{x^3} = 0 \quad (30a)$$

(b) The continuity equation:

$$\frac{d}{dx}(\Sigma x v) = 0 \quad (30b)$$

(c) The azimuthal momentum equation:

$$v \frac{d\lambda(x)}{dx} - \frac{1}{\Sigma x} \frac{d}{dx}(x^2 W_{x\phi}) = 0 \quad (30c)$$

(d) The entropy equation:

$$\Sigma v T \frac{ds}{dx} = \frac{h(x)v}{\Gamma_3 - 1} \left(\frac{dp}{dx} - \Gamma_1 \frac{p}{\rho} \right) = Q_{mag}^+ + Q_{nuc}^+ + Q_{vis}^+ - Q^- = Q^+ - g(x, \dot{m})q^+ = f(\alpha, x, \dot{m})q^+. \quad (30d)$$

Here, we have included the possibility of magnetic heating (due to stochastic field) and nuclear energy release as well. On the right hand side, we wrote Q^+ collectively proportional to the cooling term for simplicity (purely on dimensional grounds). The quantity f is almost zero on the Keplerian disk and may be about 1 close to the horizon (unless Comptonization is included which drains energy out of this region). Here,

$$\Gamma_3 = 1 + \frac{\Gamma_1 - \beta}{4 - 3\beta}; \Gamma_1 = \beta + \frac{(4 - 3\beta)^2(\gamma - 1)}{\beta + 12(\gamma - 1)(1 - \beta)} \quad (31)$$

and $\beta(x)$ is the ratio of gas pressure to total (gas plus magnetic plus radiation) pressure:

$$\beta(x) = \frac{\rho k T / \mu m_p}{\rho k T / \mu m_p + \bar{a} T^4 / 3 + B(x)^2 / 4\pi} \quad (32)$$

Here, the radial distance x is in units of $2GM_{BH}/c^2$, $B(x)$ is the strength of magnetic field in the flow, p and ρ are the gas pressure and density respectively, Σ is the density integrated in vertical direction, T is the temperature of the flow (proton and electron), $h(x)$ is the height of the flow chosen to be in vertical equilibrium, \bar{a} is the Stefan's constant, k is the Boltzmann constant, μ is the electron number per particle (and is generally a function of x in case of strong nucleosynthesis effects), m_p is the mass of the proton. Two temperature solutions are important in the case where strong cooling is present [20]. In an optically thick gas, the cooling is governed by black body emission, while in optically thin limit it could be due to bremsstrahlung, Compton effects, synchrotron radiation etc. (see, [57]). Except for Compton scattering, other coolings are computed analytically and is very simple to take care of. A novel method to include Compton cooling in accretion flows (first used in [20]) is to fit analytical curves of the numerical results of Sunyaev & Titarchuk [16] for the cooling function as a function of the optical depth:

$$g(\tau) = (1 - \frac{3}{2}e^{-(\tau+2)})\cos \frac{\pi}{2}(1 - \frac{\tau}{\tau_0}) + \frac{3}{2}e^{-(\tau+2)}, \quad (33)$$

where, τ_0 is the total Thomson optical depth of the CENBOL region and by construction $g(\tau_0) = 1$. This is easily translated in radial coordinate for a typical flow model and used in the energy equation 30(d).

The general procedure of solving this set of simultaneous differential equations is provided in [25] and in [5] in detail. Although the flow deviates from a Keplerian disk to pass through a sonic point, and therefore the sonic point properties are to be obtained a posteriori, it is best to assume the location of the sonic point as well as the angular momentum at that point (or, alternatively at the horizon) along with a suitable viscosity parameter. The solutions are integrated outward till they reach a Keplerian disk. This way the shock-free solutions are obtained. Most of the 'shock-free' solutions which pass through the outer saddle type sonic points do pass through shocks and then through the inner sonic points on their way to black holes and neutron stars. (Careless computations usually miss these solutions.) To search for solutions which include shocks, one has to incorporate Rankine-Hugoniot conditions.

The complete solutions from regions $\mathcal{E} \geq 0$ with and without shocks cannot join with a cold Keplerian flow even when viscosity is added, since these flows are not bound. If one writes the net energy (Bernoulli constant)

as

$$\mathcal{E} = \frac{1}{2}v^2 + \frac{1}{2}\frac{l^2}{x^2} + \frac{1}{\gamma - 1}a_s^2 - \frac{1}{2(x - 1)} \quad (34)$$

our arguments will be clearer. (Here, the rest mass energy in \mathcal{E} has not been included. a_s is the adiabatic sound speed). For a cold Keplerian disk, sound speed $a_s \sim 0$, $v \sim 0$, and $l_K = \frac{1}{2}\frac{x^3}{(x-1)^2}$. At the junction point, where the advective disk meets the Keplerian disk, $l = l_K$ and $\mathcal{E} = \frac{(2-x)}{4(x-1)^2} < 0$ for all $x > 2$. Only when the disk is very hot ($1 > a_s \gg 0$), or the flow is away from the equatorial plane (where potential energy is smaller than its value on the equatorial plane) or matter coming out of cold disks and eventually heated up by, say, magnetic flares or dissipation, can have specific energy larger than 0 and can join with the advective disk solutions. Note that these hot, energy conserving solutions are for strictly inviscid flow. The entire energy of the flow is advected to the black hole rendering the disk to be non-luminous. It is proposed that this may be the reason why our galactic center is also faint in X-rays [6], although arguments based on total luminosity is usually not a full proof. It is interesting that the same set of equations 30(a-d) shows a rich variety of time dependent behaviour. The implications would be discussed in the next Section.

Complete set of topologies of the viscous solutions are presented in [25] for isothermal flows. They remain identical even when the assumption of isothermality is dropped [5, 6]. For the sake of completeness of the review we reproduce here some of the selected solutions of [25] already presented in Chakrabarti [58]. Typical solutions are shown in Fig. 6(a-d) and the corresponding angular momentum (λ) distributions are shown in Fig. 6(e-h). Each solution is identified by only three parameters, namely, the inner sonic point r_{in} , the specific angular momentum at the sonic point λ_{in} and the constant viscosity parameter α . The closed solutions of Fig. 4 open up in presence of viscosity. For low enough viscosity, shock condition may still be satisfied as in Fig. 6a, but as α is increased (6b), λ_{in} is reduced (6c), or r_{in} is reduced, the topologies change completely. The open solution passing through the inner sonic point joins with a Keplerian disk at r_K . This change of topology triggered by the variation of viscosity may be considered the singlemost important development in the study of the accretion processes in the recent past. For a given cooling process (mainly governed by the accretion rate) r_K strongly depends on viscosity: higher the viscosity, smaller

is r_K . The paradoxical property is primarily responsible for the observed nature of the novae outbursts [23] as well as hard and soft states of black holes. Similar situation occurs if parameters are taken from the region I^* where only inner sonic point is present. The outer sonic point is also present for flows with positive specific energy, and thus, in principle, the solutions passing through the outer sonic point may also join with a Keplerian disk. However, we suspect that in absence of stable shock solutions, flows in 6(b-d) would produce unstable oscillatory behaviour. The region between the Keplerian disk and the black hole is basically freely falling, till close to the horizon ($x \sim l^2$; note that angular momentum is nearly constant close to the black hole) where the centrifugal barrier is formed and matter slows down, heats up and is puffed up just like a constant angular momentum thick disk. Highly viscous Keplerian disk stays in the equatorial plane till r_K and then becomes sub-Keplerian (a part of the flow may also become super-Keplerian before becoming sub-Keplerian, [5]) as the flow enters through the horizon. If the viscosity monotonically decreases with height, the flow would separate out of a Keplerian disk and form sub-Keplerian halo at a varying distance depending on the viscosity coefficient $\alpha(z)$. Thus, typically a generalized accretion disk would have the shape as shown in Fig. 3(c). The centrifugal barrier closer to the horizon may or may not be abrupt, depending on the parameters involved. In either case, the flow density, temperature, velocity etc. remain very similar as is shown in Fig. 7, where two solutions, one with and the other without a shock are plotted. Thus the properties of CENBOL is independent of whether a shock actually forms or not. For comparison, a high viscosity flow solution is also presented which deviates from a Keplerian disk closer to the black hole.

In passing, we may mention that apart from Rankine-Hugoniot (non-dissipative) shocks, global solutions also exist where the shocks themselves dissipate a large chunk of the flow energy. An infinite number of such one parameter family of dissipative shock solutions are in the literature [59]. Shock solutions in various advective disk models have also been obtained by several authors quite independently [49, 53-54, 60] with similar properties.

3 Behaviour of Matter Around a Black Hole: Results of Numerical Experiments

One of the most convincing ways to check if the inviscid and viscous solutions were stable or not is to perform numerical simulations (with a reliable code, of course!). Recently, all possible fully time dependent behaviour of the advective disks have been found [50-51, 56, 60-63]. Shock solutions (from the region SA in Fig. 4) were found to be stable and the results are in good agreement with theoretical predictions. Indeed, present development may be considered to be the best known way to test a code in spherical and cylindrical coordinates when shocks are present. Figure 8 shows the theoretical and numerical simulation results where the results from three completely different methods (smoothed particle hydrodynamics, total variation diminishing and explicit/implicit code). This development is to be compared with the poor matching of the solutions in early days of numerical simulations [64] when both the theory as well as the code were not satisfactory. Shocks also form in two dimensional (axisymmetric thick) flow very near the predicted locations. When the solutions have one sonic point and shocks are not predicted (in regions O and I) shocks do not form (uppermost and lower most sets of curves). When the solutions have two sonic points but still shocks do not form (in region NSA of Fig. 4), the shocks may form nevertheless, but they oscillate back and forth thereby changing the size of the CENBOL [50]. In presence of cooling effects, shocks may oscillate even when stable shocks are theoretically predicted [65]. This typically happens when the cooling time scale roughly agrees with the infall time scale. The oscillating shock has the period comparable to the cooling time and is believed to explain the quasi-periodic oscillations observed in the black hole candidates. The viscous flows also show the similar oscillations [63]. We suspect that whenever accretion rates of a black hole change substantially (such as when a black hole changes its spectral state), the oscillations may be set in as a result of competition among various time scales. It is generally the case that shocks are ‘always’ formed whenever some angular momentum is present! They may or may not be stable, i.e., they may be transient and propagate away to a large distance, or, they may be oscillatory, or, they may be standing. The exact behavior depends on the flow parameters.

One of the intriguing questions remained: Although advective solutions

produce sub-Keplerian flows from a Keplerian disk, are they really stable? Chakrabarti et al. [62] provides a collection of numerical simulation results including the formation of an advective disk from a Keplerian one far away from the black hole (and not just near the horizon as in [47]). Figure 9a shows the ratio of the disk angular momentum to the Keplerian angular momentum in one of the simulations. The shape is typical of such advective flows (See Fig. 10 of [20]) although the transition from Keplerian to the advective disk is not very *smooth*. At a first sight, the reason seems to be due to the fact that the derivative dl/dr in an advective flow is different from that in the Keplerian disk. One could find a smoother transition by adjusting viscosity and cooling effects at the transition. Figure 9b shows the deviation of angular momentum of a flow which included a standing shock. Apart from a mild kink in the distribution at the shock location, the flow is perfectly smooth, transonic and stable.

4 Behaviour of Matter and Stars Around a Black Hole: Observations

4.1 From Spectral Properties

Black holes are being fundamentally black, their proper identifications must necessarily include quantification of very special spectral signatures of radiating matter entering in them. The inner boundary condition of the flow is unique and this automatically separates the true solution from a large number of spurious solutions. Because of this, the spectral properties of the flow entering in a black hole should be different. The problem lies in quantification of this special character. Here we present a few observational results and how they may be readily understood using theoretical results presented in the earlier Section. The advantage of this approach is that the explanations are general (as they are straight from solutions of governing equations), and do not depend on any particular black hole candidate. In what follows, the accretion rates are expressed in units of the Eddington rate.

4.1.1 Hard and Soft states and triggering of their transitions

Galactic black holes are seen basically in two states. In soft states, more power is in soft X-rays and in hard states more power is in hard X-rays. (The extragalactic cases such state separation is not obvious, since the observations are poorer, and transition of states may take place in thousands of years. Some of the carefully observed cases the spectral nature was found to be similar to those of the galactic candidates, e.g., MRK841 [66]. Fig. 10(a-c) shows a comparison of the schematic spectra of a black hole candidate both in hard and soft states and a neutron star candidate. Generally, neutron star spectra are composed of a multicolour black body component coming out of a Keplerian disk and a black body component coming out of the stellar boundary layer. They always show soft bumps, unlike in a black hole in hard states, where the soft bump disappears. A neutron star does not show the weak power-law component which is really the hallmark of a black hole in soft states. The explanation of this apparently puzzling state variation may be simple: the Keplerian and sub-Keplerian components redistribute matter among themselves depending on viscosity of the flow which, at the same time, also change the inner-edge of the Keplerian component. Sudden rise in viscosity would bring more matter to the Keplerian component (with rate \dot{m}_d) and bring the Keplerian edge closer to the black hole (see, [47] for numerical simulation of this effect) and sudden fall of viscosity would bring more matter to sub-Keplerian halo component (with rate \dot{m}_h) and takes away the Keplerian component away. Disk component \dot{m}_d not only governs the soft X-ray intensity directly coming to the observer, it also provides soft photons to be inverse Comptonized by sub-Keplerian CENBOL electrons. The CENBOL (comprised of matter coming from \dot{m}_d and \dot{m}_h) will remain hot and emit power law (energy spectral index, $F_\nu \sim \nu^{-\alpha}$, $\alpha \sim 0.5 - 0.7$) hard X-rays only when its intercepted soft photons from the Keplerian disk (See Fig. 4) are insufficient, i.e., when $\dot{m}_d \ll 1$ to $\dot{m}_d \sim 0.1$ or so, while \dot{m}_h is much higher. For $\dot{m}_d \sim 0.1 - 0.5$ (with $\dot{m}_h \sim 1$), CENBOL cools catastrophically and no power law is seen (this is sometimes called a high state). With somewhat larger \dot{m}_d , the power law due to the bulk motion of electrons [20, 67-68] is back at around $\alpha \sim 1.5$ (this is sometimes called a very high state). Figure 11 (taken from [21]) shows a typical hard to soft state transition as \dot{m}_d is increased. Here, power $EF(E)$ is plotted against the energy E of the emitted photons. The dashed curve drawn for $\dot{m}_d = 1.0$

includes the convergent flow behaviour of the inner part of CENBOL. Details of the solutions are in [20, 21, 23]. Such hard/soft transitions are regularly seen in black hole candidates [69-73].

4.1.2 Constancy of Slopes in Hard and Soft States

Spectra of the advective disk solutions show a remarkable property: the slope $\alpha \sim const$ in hard states even when \dot{m}_d is increased by a factor of a thousand. The degree of constancy is increased [21] if one assumes that as the viscosity changes, the matter is actually redistributed between the Keplerian and sub-Keplerian halo components rather than assuming that both the components are completely independent. This constancy of slopes is regularly seen [20, 23, 72, 74-75]. Particularly important is the weak power law in the soft state as this is not observed in neutron star candidates. CENBOL around neutron stars may also cool down to produce soft state for the same reason. However, they can go up to high state and not up to ‘very high’ state where the weak power law due to convergent flow is seen. In bulk motion Comptonization bulk momentum of the quasi-freely falling electrons (outside the horizon) are transported to the soft photons (Doppler Effect – [20, 67-68]). This effect becomes important (compared to the thermal Comptonization) when the electrons themselves are cool (less than a few keV). In neutron stars, electrons slow down on the hard surface due to radiation forces opposite to gravity acting on them, and therefore the bulk momentum transfer is negligible. Thus black holes could be identified by spectral signatures alone provided they are seen in soft states [4, 20].

4.1.3 Variation of Inner Edge of the Keplerian Component

This is a trivial property of the advective disks (see, [5, 20]). As viscosity is increased, the location r_K where the disk deviates from Keplerian is *generally* decreased if other two parameters (r_{in} and l_{in}) are held fixed. Thus, in hard states, not only \dot{m}_d is smaller, the r_K is also larger. As the viscosity increases, r_K becomes smaller in viscous time scale, at the same time more matter is added to the Keplerian component. This behaviour is also seen in black hole candidates [76]. In advection dominated models of Narayan & Yi [27] such variations are achieved by evaporation of the disks by unknown fundamental physics.

4.1.4 Rise and Fall of X-ray Novae

X-rays novae (e.g., A0620-00, GS2000+25, GS1124-68, V404 Cygni etc.) produce bursts of intense X-rays which decay with time (decay time is typically 30d). This phenomenon may be repeated every tens to hundreds of years. While in persistent black hole candidates (such as Cyg X-1, LMC X-1, LMC X-3) Keplerian and sub-Keplerian matter may partially redistribute to change states (see Section 3 above), in X-ray novae candidates the net mass accretion rate may indeed decrease with time after the outburst, even if some redistribution may actually take place. First qualitative explanation of the change of states in X-ray novae in terms of the advective disk model was put forward by ETC96. The biggest advantage of the advective solution is that it automatically moves the inner edge of the Keplerian disk as viscosity is varied. Similar to the dwarf novae outbursts, where the Keplerian disk instability is triggered far away (e.g., [77]) here also the instability may develop and cause the viscosity to increase, and the resulting Keplerian disk with higher accretion rate moves forward. In [21], several such spectral evolutions have been presented. In Fig. 12, one such case is shown, where the increase in viscosity is used to cause the decrease in r_K from 9000 to 10, keeping $\dot{m}_h = 1$ and $\dot{m}_d = 0.01$. As the inner edge goes from 9000 to 5000, the optical (around tens of eV) peaks first, which is followed by hard X-rays (at around hundreds of keV) till r_K reaches about several hundred Schwarzschild radii. After that the hard X-ray subsides and soft X-ray intensifies. The optical precursor of an X-ray nova GRO J1655-40 have been seen recently [78].

4.1.5 Quiescent States of X-Ray Novae Candidates

After years of X-ray bursts the novae becomes very faint and hardly detectable in X-rays. This is called the Quiescent states of the black holes. This property is built in Advective disk models. As already demonstrated [5, 20], r_K recedes from the black holes as viscosity is decreased. With the decrease of viscosity, less matter goes to the Keplerian component [47], i.e., \dot{m}_d goes down. Since the inner edge of the Keplerian disk does not go all the way to the last stable orbit, optical radiation is weaker in comparison with what it would have been predicted by a Shakura-Sunyaev [11] model (see, plots for $r_K = 9000$ and 8000 for such spectral behaviour

in Fig. 12 above). This behaviour is seen in V404 Cyg [79] and A0620-00 [80]. The deviated component from the Keplerian disk almost resembles a constant energy rotating flow described in detail in [3]. It is also possible that our own galactic center may have this low viscosity, low accretion rate with almost zero emission efficiency [3] global advective disks as mentioned in [6].

Recently, a so-called advection dominated model has been used to fit these states [81]. Though it is supposed to be an off-shoot of the advective disk solutions for low optical depth limits, this is not a self-consistent model. In this model highly viscous ($\alpha \sim 0.1 - 0.5$) quasi-spherical flow resulted from Keplerian disk evaporation (which is also in equipartition with magnetic field at all radii!) was used. The data contained typically ‘one point’ in the hard X-ray region and fits are poor. On the contrary, advective disk solution [3, 5, 20] does not require such evaporation, and the advecting ion torus of low mass accretion rate comes most naturally out of the governing equations only for very low viscosity case. The deviation from a Keplerian takes place several thousand Schwarzschild radii. In high viscosity case angular momentum transport rate becomes so high that the flow deviates from a Keplerian disk almost immediately from the inner sonic point. Advecting disks produce the quiescent state like spectra [20-21] without making any further unwarranted approximations, regarding magnetic equipartition, etc. However, so far, advective disk solutions, theoretically complete as they are, have not made any serious attempt to fit observational data yet.

4.1.6 Quasi-Periodic Oscillations of X-rays

As mentioned in Section 2.4, in some large region of the parameter space the solutions of the governing equations 30(a-d) are inherently time-dependent. Just as a pendulum inherently oscillates, the physical quantities of the advective disks also show oscillations of the CENBOL region for some range in parameter space. This oscillation is triggered by competitions among various time scales (such as infall time scale, cooling time scales by different processes). Thus, even if black holes do not have hard surfaces, quasi-periodic oscillations could be produced. Although any number of physical processes such as acoustic oscillations [82], disko-seismology [83], trapped oscillations [84], could produce such oscillation frequencies, modulation of 10 – 100 per cent or above cannot be achieved without bringing in the dynamical partici-

pation of the hard X-ray emitting region, namely, the CENBOL. By expanding back and forth (and puffing up and collapsing, alternatively) CENBOL intercepts variable amount of soft photons and reprocesses them. Some of the typical observational results are presented in [85-87]. Recently more complex behaviour has been seen in GRS 1915+105 [88-89], which may be understood by considering several cooling mechanisms simultaneously. Particularly interesting is the observations [88] that the rise time is slow (10-15s) but the decay time is rapid (2-3s). This is typically interpreted as the signature of rapid swallowing of matter into a black hole. QPOs in neutron stars do not show this property. Some chaotic behaviour of r_K under non-linear feed back mechanism cannot be ruled out either.

4.1.7 Nature of the Iron Line

Resonance lines of iron have been seen in several black hole candidates [90, 91]. Usually one of the two observed wings is found to be stretched compared to the other and it is explained to be due to the combination of the Doppler shift and the gravitational red-shift. Generally, it is difficult to explain very large equivalent width of the lines in this models. This problem can be circumvented if the lines are assumed to be coming from outflowing winds. The stretched wing would then be due down-scattered emission lines [20]. The idea of line emissions from the winds is finding supports by other workers as well [91-93].

4.2 From Motion of Stars

Measurements of the stellar rotation and velocity dispersion profiles close to a galactic nucleus can provide the mass of the central body. For a spherical distribution of stars, for instance, virial mass within radius is obtained as $M(R) = \frac{\beta \sigma_r^2 R}{G}$, with β varying from 2 to 3. Using the dispersion and rotation, Kormendy [94] computed the mass of the central nucleus of M31 to be a few $\times 10^7 M_\odot$. Its companion M32 was probably the first galaxy with a convincing evidence of a massive black hole of about $3 \times 10^6 M_\odot$ (see, [95] and references therein). Our own galactic center is now being studied extensively by Genzel group [96]. The projected stellar velocity dispersion increases significantly from 55 km s^{-1} at around 5pc, to 180 km s^{-1} at around 0.1pc. The estimated mass is $2.5 - 3.2 \times 10^6 M_\odot$. The corresponding mass density is more than

$6.5 \times 10^9 M_\odot \text{pc}^{-3}$. This is one of the highest observed concentration of matter that has been detected so far.

4.3 From Mass Functions

Some argue that measurement of the central mass is the most definite way to identify a black hole. In a binary system, the mass of the compact primary m_1 is estimated from the observed mass function $f(m)$ and the inclination of the orbital plane i (e.g., [1]):

$$M_1 = \frac{f(m)(1+q)^2}{\sin^3 i} \quad (35)$$

Since M_1 is the minimum mass of the compact object, if its value is larger than $3M_\odot$, the object is most probably a black hole. satisfy these criteria and the compact components are possibly a black holes. The most well studied suspected black hole component Cyg X-1 (1956+350) has mass function of only $0.24M_\odot$ and therefore it fails this criterion. However, spectral signatures, such as the transition of states [73, 97] and weak hard tail in the soft state positively identify it to be a black hole.

4.4 From Doppler Shifts

As matter rotates around a black hole, the line emissions produce well known double horned pattern seen in disks around compact stars. The origin of this spilt lies in the Doppler effect. Here the frequency of matter increases as matter comes towards an observer and it decreases as matter goes away from an observer. The change of frequency is roughly $\delta\nu/\nu \sim v/c$, where v is the rotational velocity projected along the line of sight. In a Keplerian disk, $v_K = \sqrt{GM/x}$. Thus knowing where the line is actually emitted, one could compute the mass of the central object. Through water mega-maser experiments one has been able to detect this strictly Keplerian motion in NGC4258 [98] and the estimated mass of the central black hole is $4 \times 10^7 M_\odot$. Observation of the disk around M87 was made using Hubble space telescope and the Doppler shift is clearly observed in flows within the disk. Estimate of the mass of the black hole assuming a Keplerian disk is around $(2.0 \pm 0.9) \times 10^9 M_\odot$ [99]. However, the interpretation of the Doppler shift varies. It is doubtful whether the lines could be emitted at large distances ($\sim 20 - 80$

thousand Schwarzschild radii from the center) from a Keplerian disk, as the disk would be too cold (unless the disk is strongly warped as NGC4258, and intercepts its own X-rays emitted at the center of the galaxy; though M87 is not considered to be particularly bright in X-rays). An alternate explanation would be that the line emission farther away from the center is (spiral-)shock excited. However, flows with spiral shocks (any shocks for that matter) must be at least partially sub-Keplerian (even if pre-shock flow is Keplerian, post-shock flow must be sub-Keplerian for any shock strength) and therefore the estimated mass from the same shift in frequency must be higher. This suggestion produces a mass of much higher value [100] – $4 \pm 0.2 \times 10^9 M_\odot$ within $10^4 R_g$, i.e., about 3.5pc. This is the first time where, using the suggestion of even a partially sub-Keplerian disk in galaxies, higher central black hole mass estimate has been made. It was farther noted that the spiral shock should not be extended below 3.5pc, otherwise, the width of the lines would be higher. Recently, Macchetto et al. [101] did find this deviation from Keplerian in the outer edge of the disk. However, central of this disk is very close to Keplerian. Using high resolution (0.09”) observation of Hubble Space Telescope in this region they also found the mass to be in this high range ($3.2 \pm 0.9 \times 10^9 M_\odot$). Thus, results from Keplerian and sub-Keplerian regions independently give rise to the same high black hole mass. Another object whose mass has been obtained recently using Doppler effect is M84. Long-slit spectrophotometry is used in mapping the velocity profile across the disk and assuming a Keplerian disk, the mass is found to be $1.5 \times 10^9 M_\odot$ [102].

4.5 From Reverberation Mapping

Generally, active galactic nuclei also show line emissions along with continuum emissions. These lines are believed to be emitted from rapidly moving clouds on either sides of an accretion disk. Measurement of the motion of the cloud from Doppler shift and the distances of the cloud from reverberation mapping [103] method can give an estimate of the mass of the central object. In this method, the time lag between certain variation in the continuum spectra and the line emission is used to measure the distance of the broad line emitters. Masses of a few active galaxies have been measured this way: NGC 5548 ($8.8 \times 10^7 M_\odot$), NGC 3227 ($3.8 \times 10^7 M_\odot$) etc.

4.6 Comparative Studies of Detection Mechanisms

There are several ways such as those using motion of stars, Doppler effects, mass function, spectral features, gravitational wave (which has not been detected yet) etc., for the identification of a black hole. Except for the spectral feature study (that too, for instance, in the very soft state where the weak power-law region is observed) and the gravitational wave signals, where the effect of the horizon could be seen, all the other criteria cannot really distinguish a black hole (with a horizon) from another hypothetical solution of Einstein equation which is massive and ‘somehow’ compact. In several cases, particularly, in the cases of active galaxies, one may have to be satisfied with the more indirect methods such as Doppler shifts, reverberation mapping etc. since transition of states from hard to soft, or vice versa, might take a very *long* time.

5 Signatures of Advective Flows in Other Branches of Astrophysics

If the flow is highly advective around a black hole, and at the same time shock structures and CENBOL form, as the solutions seem to indicate, there are a large number of spin-offs which should also be observable. For instance, jets and outflows are known in many systems. Are they related to the degree by which the flow is sub-Keplerian or the formation of CENBOL? If so, can the outflow rate be estimated from such considerations? Similarly, since the temperature of the advective disks is very high, could it cause a significant nuclear burning in the disks? Could the non-Keplerian disk influence gravitational wave emission from a coalescing companion which happens to interact with the disk as well? There answers seem to be ‘yes’ to all, and major developments in these directions have been done very recently. We discuss them here very briefly.

5.1 Physics of Jets: Estimation of the Outflow Rate From an Advective Flow

Outflows are common in many astrophysical systems which contain black holes and neutron stars. Difference between stellar outflows and outflows

from these systems is that the outflows in these systems have to form out of the inflowing material only, whereas in stars outflows are ‘extensions’ of the staller atmosphere. Although a black hole does not have a hard surface, the centrifugal barrier behaves like one, and therefore mass loss associated with it could be computed. Of course, a shock surface around a black hole need not be only centrifugally supported. Chang & Ostriker [104] produced shocks assuming considerable pre-heating of the incoming flow and Kazanas & Ellison [105] suggested shock formation which are supported by pair plasma pressure. As long as such a region where some compression (other than geometric, with shock or no shock) is formed in the inflow, the jet formation take place. It is to be noted that production of jets have always been found to be favourable when the disk itself is sub-Keplerian [106].

Figure 13 shows schematically the ‘black box’ where outflows are generated. Assuming this configuration, mass loss is estimated very easily [107]. The procedure involves in first computing the CENBOL temperature T_s from the incoming flow using steady shock condition and then use the same procedure as used on stellar surface, namely, mass loss from this surface using transonic flow condition. The ratio of outflow rate to the inflow rate in terms of the compression ratio R of gas turns out to be,

$$R_{\dot{m}} = \frac{\dot{M}_{out}}{\dot{M}_{in}} = \frac{\Theta_{out}}{\Theta_{in}} \frac{R}{4} \exp(-f) f_0^{3/2} \quad (40)$$

where, $f = f_0 - \frac{3}{2}$ and $f_0 = (2n + 1)R/(2n)$ [$n = (\gamma - 1)^{-1}$ is the polytropic constant.]. Notice that this simple result does not depend on the location of the sonic point or shock (namely the size of the dense cloud, and physical process which produces it) or the outward force causing the mass loss. It is a function of compression ratio R for a given geometry. In a relativistic inflow $n = 3$, $\gamma = 4/3$ and $R = 7$ and the ratio of inflow and outflow becomes,

$$R_{\dot{m}} = 0.052 \frac{\Theta_{out}}{\Theta_{in}} \quad (41a)$$

and for inflow of an ionized gas $n = 3/2$, $\gamma = 5/3$ and $R = 4$, and the ratio in this case becomes,

$$R_{\dot{m}} = 0.266 \frac{\Theta_{out}}{\Theta_{in}} \quad (41b)$$

Outflows are usually concentrated near the axis, while the inflow is near the equatorial plane. Assuming a half angle of 10° in each case, we obtain,

$$\Theta_{in} = \frac{2\pi^2}{9}; \quad \Theta_{out} = \frac{\pi^3}{162} \quad (42)$$

and

$$\frac{\Theta_{out}}{\Theta_{in}} = \frac{\pi}{36}. \quad (43)$$

The ratios for $\gamma = 4/3$ and $\gamma = 5/3$ are then

$$R_{\dot{m}} = 0.0045 \quad \text{and} \quad R_{\dot{m}} = 0.023 \quad (44)$$

respectively. This is to be compared with the rate $R_{\dot{m}} = 0.004$ found in radiation dominated flow [108]. A more exact computation of the mass loss rate could be done using exact transonic solutions for the inflow and outflow [109]. Fig. 14, shows the actual solution of isothermal winds coming out of adiabatic accretion for a rotating flow with $\lambda = 1.89$ and $\mathcal{E} = 0.0038$. Three outflowing dashed curves correspond to three accretion rates (decreasing monotonically from the upper curve to the lower one). In this calculation, the outflowing region is assumed to be between the centrifugal barrier and the funnel wall, and the Comptonization (Chakrabarti & Titarchuk, 1995) has been qualitatively incorporated to compute the CENBOL temperature as a function of the accretion rate. The general conclusion in this case is that the percentage of the outflow rate is non-linearly dependent on the inflow rate even for a constant angular momentum flow, since the temperature of the CENBOL which drives the flow is a steep function of \dot{M}_{in} . For lower accretion rate, the Comptonization is inefficient and the ratio of outflow to inflow increases.

5.2 Nuclear astrophysics: Nucleosynthesis in advective disks around black holes

Chakrabarti [110] and Chakrabarti, Jin & Arnett [111], first pointed out that a considerable nucleosynthesis could take place during the infall and heavier elements may be produced inside the thick disk, a fraction of which could be ejected out through bipolar outflows and jets [112]. Although the disk model used was very preliminary (basically then fashionable purely rotating thick

accretion disk with a slow infall) the conclusions were firm and were verified by a large number of independent workers [113-114] using other disk models.

In the decade since these works were initiated, the self-consistent advective disk model has been developed. This motivates one to look into the nucleosynthesis problem once more, specially when the shocks and CENBOL regions are also included in the computation. Fig. 15 shows the variation of the abundance as the matter enters the advective disk regime [115]. Here a $10M_{\odot}$ central object and a (total: Keplerian and sub-Keplerian combined) mass accretion rate of $1\dot{M}_{Edd}$ are used. Comptonization is roughly incorporated by reducing the proton temperature by a factor of 30 as is seen in [20] in this case. The cooling factor $f = 0.5$ and viscosity $\alpha_{\text{II}} = 0.05$ were used which gave $x_K = 498r_g$. The shock is formed at $x_s = 13.9r_g$ (see, Fig. 4 for the full solutions). The dotted curves are drawn when only the supersonic branch through outer sonic point is used, while the solid curves are drawn when the solution takes more stable branch through the shock and finally through the inner sonic point. At the shock, the sudden rise in temperature as well as higher residence time in the post-shock flow causes the abundance to change abruptly although the final product at the horizon remains very similar. Only the elements with abundance above 10^{-4} at any stage during the inflow are indicated, although a total of 255 isotopes (from neutron, proton, helium to germanium) were used in the network. This is a more ‘dramatic’ case. Generally, when accretion rate is high, the advective region is small, so the effect is much weaker. When accretion rate is low, advective region is larger only when the viscosity is low also. But density being smaller, the effect (i.e., change in abundance) is also weaker.

In the high accretion rate case, heavy elements are produced and light elements are destroyed, while in the low accretion rate case, one may imagine that spallation reaction becomes important to produce some excess Li^7 [116-117]. However, detailed computation shows that before the spallation could take place, entire He^4 may be destroyed due to photo disintegration [118]. This is because, even though the accretion flow is of low rate and photons emitted by itself could be low, photons may be supplied externally by the cooler Keplerian disk. These cooler photons are energized by inverse Comptonization and they can then participate in photo-disintegration process. Thus, the production of Li^7 or D does not seem to be possible under any circumstances in the black hole accretion. One interesting physical process make the nucleosynthesis study much more important: the production

of neutron tori [119]. Neutrons produced in the advective disk due to photo-dissociation produce a neutron tori in the advective region which, mixing with fresh incoming matter may produce neutron rich isotopes of the galaxies.

The changes in abundance in the CENBOL region is important, since the wind may be produced from this region at a rate \dot{M}_{out} (see Section 5.1). Part of wind could be intercepted by the companion star and it is likely that these new elements may be detected in the stellar atmosphere. In this context, recent observations of high Lithium abundance in K-star companions of black holes [120] may be significant, although this may be entirely due to magnetic flaring on the stars [121]. and quasars, heavy elements produced in the disk may supply metallicity in the galaxies.

Jin, Arnett and Chakrabarti [122] originally concluded that the effect of nucleosynthesis is important only for very low viscosities. This is because they focused on cooler radiation dominated disks where higher residence time was required. Using present advective disks, even for $\alpha \sim 0.1 - 0.4$, nucleosynthesis seems to be important for stellar black holes [115]. For supermassive black holes the effects remain weaker since the density of the disk becomes much lower for a comparable non-dimensional accretion rate.

5.3 Gravity Wave Astronomy: Effects on Gravitational Wave Emission

Traditionally, coalescence of two compact bodies is studied in the absence of accretion disks. This may be justified where both the components in a binary are compact, such as two neutron stars and two stellar mass black holes. When a supermassive black hole at the galactic center is surrounded by an advective disk through which a compact companion star gradually moves in along an instantaneously Keplerian orbit, not only does the angular momentum of the companion is lost due to gravitational wave emission, but some angular momentum is also changed through the interaction of the non-Keplerian part of the disk with the companion. For instance, in the super-Keplerian region of the disk, the companion will *gain* angular momentum due to accretion from disk material, while in the sub-Keplerian region the companion would lose angular momentum due to accretion of negative angular momentum. In either case, the wave pattern of the emerging gravi-

tational wave would be affected. Through detailed computation it was shown that the disk effect could be up to 7–10 percent of the main effect [123]. Similar deviations from standard template is also possible when self-gravitating disk is present, since Keplerian angular momentum distribution of such disks are completely different [124].

Figure 16, shows the effect of the presence of an accretion disk on the gravity wave pattern in a binary black hole system consisting of two black holes with mass $10^8 M_\odot$ and $10^6 M_\odot$. The solution for the disk quantities is obtained from the equations 30(a-d) for parameters $\gamma = 5/3$, $\alpha = 0.02$, $f = 0.0$, $x_{in} = 2.3$, and $l_{in} = 1.7$. Accretion rate $\dot{M} = 1000\dot{M}_{Edd}$ is chosen for enhancing the effect. When \dot{M} is reduced, as is appropriate for an advective disk, the effect is proportionately smaller. In Fig. 16a, the radial distance of the companion as function of time is compared (solid curve is with the disk, and the dashed curve is without the disk), while in Fig. 16b, the ‘chirp’ profiles as functions of real time are compared (only last few Schwarzschild radii are shown). When the sub-Keplerian disk is included, the companion falls more rapidly due to enhanced loss of angular momentum.

When viscosity is large the inner edge of the Keplerian component is closer to the black hole and the soft state is achieved for higher accretion rates. For the same set of parameters, the effect on gravitational wave emission is maximum, since close to the black hole the flow would still be advective and sub-Keplerian. In the hard states, the viscosity and accretion rate is low and the inner edge of the Keplerian component is farther out. In this case, the disk will have a very little effect on the gravity wave emission. Thus, for the first time, results from electromagnetic wave and the gravitational wave could be combined to obtain a better understanding of the system parameters. Detailed computations of the templates are in progress and would be reported elsewhere.

6 Concluding Remarks

That black holes, which represent the end product of massive stars and star clusters, must exist somewhere in this universe is beyond any doubt. The issues discussed in this review were: whether they are in principle detectable, how to detect them and whether they have been detected. It seems that a few cases at least they *have been detected*. If the observations of Genzel et al.

[96, 125] is correct, then the mass of the central $0.1pc$ region of our galaxy would be $2.5 - 3.2 \times 10^6 M_\odot$ and the corresponding mass density would be $6.5 \times 10^9 M_\odot/pc^3$, the highest measured concentration so far. The water megamaser measurement of the nucleus of NGC4258 within $0.1pc$ has the central mass of $4 \times 10^7 M_\odot$ and corresponding mass density is $6.5 \times 10^9 M_\odot/pc^3$. The central mass of M87 from the estimation of Keplerian and non-Keplerian components is $\sim 4 \times 10^9 M_\odot$ and the corresponding mass density is $2.0 \times 10^7 M_\odot/pc^3$. Although, Cyg X-1 is the most studied black hole candidate so far, its mass function is very low. Its confirmation as a black hole comes from its spectral features, especially the weak power-law slope of the bulk motion Comptonization in its soft state. The only candidates with mass function higher than, say, $3M_\odot$, are *GRS1124 - 683*, *GROJ1655 - 40*, *H1705 - 250*, *GS2000 + 25* and *GS2023 + 338* and are possible stellar mass black holes. With the improvements of the future observational techniques, one needs to focus on more detailed predictions of the advective disks, such as variation of the solution topology with specific energy, or equivalently, accretion rate. With the emergence of gravitational wave astronomy, the wave signals from galactic centers should be detectable. The proposal presented in Section (5.3) would for the first time correlate the distortions of the gravitational wave signals with those from the spectral signatures. Together they would not only verify black holes, they may also become the strongest test of general relativity to date.

Reference

References

- [1] S.L. Shapiro, S.A. Teukolski 1983 *Black Holes, White Dwarfs and Neutron Stars — the Physics of Compact Objects* John Wiley & Sons, New York
- [2] H. Bondi 1952 *Mon. Not. R. Astron. Soc.* **112** 195
- [3] S.K. Chakrabarti 1989 *Astrophys. J.* **347** 365
- [4] S.K. Chakrabarti and Sahu, S. 1997 *Astron. Astrophys.* **323** 382
- [5] S.K. Chakrabarti 1996 *Astrophys. J.* **464** 646
- [6] S.K. Chakrabarti 1996 *Physics Reports* **266** No 5 & 6 229
- [7] S.L. Shapiro 1973 *Astrophys. J.* **180** 531
- [8] S.L. Shapiro 1973 *Astrophys. J.* **185** 69
- [9] S.K. Chakrabarti 1990 *Comments on Astrophys.* **4** 209
- [10] S.K. Chakrabarti and S. D’Silva 1994 *Astrophys. J.* **424** 138
- [11] N.I. Shakura and R.A. Sunyaev 1973 *Astron. Astrophys.* **24** 337
- [12] I. Novikov and K.S. Thorne 1973 in: *Black Holes* (eds.) C. DeWitt and B. DeWitt, Gordon and Breach, New York
- [13] D.M. Eardley and A.P. Lightman 1975 *Astrophys. J.* **200** 187
- [14] R.A. Sunyaev and J. Trümper 1979 *Nature* **279** 506
- [15] R.A. Sunyaev and L.G. Titarchuk 1980 *Astron. Astrophys* **86** 121
- [16] R.A. Sunyaev and L.G. Titarchuk 1985 *Astron. Astrophys.* **143** 374
- [17] A.A. Zdziarski 1985 *Astrophys. J.* **294** L79
- [18] A.A. Zdziarski 1986 *Astrophys. J.* **305** 45

- [19] A.A. Galeev, R. Rosner and G.S. Vaiana 1979 *Astrophys. J.* **229** 318
- [20] S.K. Chakrabarti and L.G. Titarchuk 1995 *Astrophys. J.* **455** 623
- [21] S.K. Chakrabarti 1997 *Astrophys. J.* **484** 313
- [22] Y. Tanaka and W.H.G. Lewin 1995 in *X Ray Binaries*, Eds. W.H.G. Lewin, J. Van Paradijs, E.P.J. Van-den Heuvel, p. 126 Cambridge University Press
- [23] . Ebisawa, L. Titarchuk and S.K. Chakrabarti 1996 *Publ. Astron. Soc. Japan* **48** No. 1
- [24] S.K. Chakrabarti 1996 *Mon. Not. R. Astron. Soc.* **283** 325
- [25] S.K. Chakrabarti 1990 *Theory of Transonic Astrophysical Flows* World Scientific Publishers (Singapore)
- [26] M.A. Abramowicz, B. Czerny, J.P. Lasota and E. Szuzkiewicz 1988 *Astrophys. J.* **332**
- [27] R. Narayan and I. Yi 1994 *Astrophys. J.* **428** L13
- [28] B. Paczyński and P.J. Wiita 1980 *Astron. Astrophys.* **88** 23
- [29] M.J. Rees, M.C. Begelman, R.D. Blandford and E.S. Phinney 1982 *Nature* **295** 17
- [30] B. Paczyński and G. Bishnovaty-Kogan 1981 *Acta Astron.* **31** 283
- [31] B. Muchotrzeb and B. Paczyński 1982 *Acta Astron.* **32** 1
- [32] E.P.T. Liang and K.A. Thompson 1980 *Astrophys. J.* **240** 271
- [33] M.A. Abramowicz and W.H. Zurek 1981 *Astrophys. J.* **246** 314
- [34] R. Matsumoto, S. Kato, J. Fukue and A.T. Okazaki 1984 *Publ. Astron. Soc. Japan* **36** 71
- [35] J. Fukue 1987 *Publ. Astron. Soc. Japan* **39** 309
- [36] A. Ferrari, E. Trussoni, R. Rosner and K. Tsinganos 1985 *Astrophys. J.* **294** 397

- [37] R. Narayan and I. Yi 1995 *Astrophys. J.* **444** 231
- [38] R. Narayan 1998 in *Accretion Phenomenon and Related Outflows*, Eds. D. Wickramasinghe, L. Ferrario & G. Bicknell.
- [39] X.M. Chen, M.A. Abramowicz, J.-P. Lasota 1997 *Astrophys. J.* **476** 61
- [40] R. Narayan, S. Kato and Honma, F. 1997 *Astrophys. J.* **476** 49
- [41] F. Haardt and L. Maraschi 1991 *Astrophys. J.* **380** L51
- [42] F. Haardt and L. Maraschi 1993 *Astrophys. J.* **413** 507
- [43] C.W. Misner, K.S. Thorne and J.A. Wheeler 1973 *Gravitation* (Freeman: San Francisco)
- [44] M. Anderson and J.P.S. Lemos 1988 *Mon. Not. R. Astron. Soc.* **233** 489
- [45] J.I. Castor, D.C. Abbott and R.I. Klein 1975 *Astrophys. J.* **195** 157
- [46] R.A. Flammang 1982 *Mon. Not. R. Astron. Soc.* **199** 833
- [47] S.K. Chakrabarti and D. Molteni 1995 *Mon. Not. R. Astron. Soc.* **272** 80
- [48] S.K. Chakrabarti 1989b *Publ. Astron. Soc. Japan* **41** No. 6 1145
- [49] J.F. Lu and F. Yuan 1997 *Publ. Astron. Soc. Japan* **49** 525
- [50] D. Ryu, S.K. Chakrabarti and D. Molteni 1997 *Astrophys. J.* **474** 378
- [51] S.K. Chakrabarti and Molteni D. 1993 *Astrophys. J.* **417** 671
- [52] K. Nakayama 1992 *Publ. Astron. Soc. Japan.* **259** 259
- [53] K. Nobuta and T. Hanawa 1994 *Publ. Astron. Soc. Japan* **46** (1994) 257
- [54] R. Yang and M. Kafatos 1995 *Astron. Astrophys.* **295** 238
- [55] S.K. Chakrabarti and P.J. Wiita 1992 *Astrophys. J.* **387** L21
- [56] D. Molteni, G. Lanzafame and S.K. Chakrabarti 1994 *Astrophys. J.* **425** 161

- [57] G.B. Rybicki and A.P. Lightman 1979 *Radiative Processes in Astrophysics* John Wiley & Sons (New York)
- [58] S.K. Chakrabarti 1997 in *Black Holes: Theory and Observations* (Ed.) F. Hehl, Springer Verlag
- [59] M.A. Abramowicz and S.K. Chakrabarti, 1990 *Astrophys. J.* **350** 281
- [60] J.F. Lu, K.N. Yu, F. Yuan and E.C.M. Young 1996 *Astron. Astrophys.* **321** 665
- [61] D. Molteni, D. Ryu and S.K. Chakrabarti 1996 *Astrophys. J.* **470** 460
- [62] S.K. Chakrabarti, D. Ryu and D. Molteni, H. Sponholz, G. Lanzafame and G. Eggum 1996 in the *Proceedings of the IAU Asia-Pacific regional meeting* (Eds.) H.M. Lee, S.S. Kim, K.S. Kim, *J. Korean Astron. Soc.* **29** 229
- [63] G. Lanzafame, D. Molteni, S.K. Chakrabarti 1998 *Mon. Not. R. Astron. Soc.* (in press).
- [64] J.W. Hawley, L.L. Smarr and J.R. Wilson 1984 *Astrophys. J.* **277** 296
- [65] D. Molteni, H. Sponholz and S.K. Chakrabarti 1996 *Astrophys. J.* **457** 805
- [66] K. Arnaud, et al. 1986 *Mon. Not. R. Astron. Soc.* **217** 105
- [67] R.D. Blandford and D.G. Payne 1982 *Mon. Not. R. Astron. Soc.* **199** 883
- [68] L.G. Titarchuk, A. Mastichiadis and A. Kylafis 1997 *Astrophys. J.* **487** 834
- [69] J.F. Dolan, C.J. Crannel, B.R. Dennis, K.J. Frost and L.E. Orwig 1979 *Astrophys. J.* **230** 551
- [70] S. Miyamoto, K. Kimura, S. Kitamoto, T. Dotani and K. Ebisawa 1991 *Astrophys. J.* **383** 784
- [71] M. Ricketts 1983 *Astron. Astrophys.* **118** L3

- [72] K. Ebisawa, M. Ogawa, T. Aoki, T. Dotani, M. Takizawa, Y. Tanaka, K. Yoshida and Miyamoto S. 1994 *Publ. Astron. Soc. Japan.* **46** 375
- [73] S.N. Zhang, W. Cui, B.A. Harmon, W.S. Paciesas, R.E. Remillard and J. van Paradijs 1997 *Astrophys. J.* **477** L95
- [74] R.A. Sunyaev, et al. 1994 *Astron. Lett.* **20** 777
- [75] S. Kuznetsov, et al. 1997 *Mon. Not. R. Astron. Soc.* (in press)
- [76] M. Gilfanov, E. Churazov, R.A. Sunyaev 1997, in *Accretion Disks – New Aspects*, (Eds.) E. Meyer-Hofmeister & H. Spruit, Springer (Heidelberg).
- [77] J. Cannizzo 1993 in *Accretion Disks in Compact Stellar Systems* (Ed.) J. C. Wheeler, World Scientific: Singapore
- [78] J.A. Orosz, R.A. Remillard, C.D. Bailyn and McClintock, J.E. 1997 *Astrophys. J.* **478** 830
- [79] R.M. Wagner, S.G. Starrfield, R.M. Hjellming, S.B. Howell, and T.J. Kreidl, 1994 *Astrophys. J.* **401** L97
- [80] J.E. McClintock, K. Horne and R.A. Remillard 1995 *Astrophys. J.* **442** 358
- [81] R. Narayan, D. Barret and J.E. McClintock *Astrophys. J.* 1997 **482** 448
- [82] R. Taam, X.M. Chen and J. Swank, 1997 *Astrophys. J.* **485** L83
- [83] M. Nowak and R.V. Wagoner, 1993 *Astrophys. J.* **418** 183
- [84] S. Kato, F. Honma and R. Matsumoto, 1988 *Publ. Astron. Soc. Japan* **40** 709
- [85] Y. Dotani 1992 in *Frontiers in X-ray Astronomy*, Eds. Y. Tanaka, & K. Koyama, K. p. 152 Universal Academy Press, Tokyo
- [86] J. Halpern and H.L. Marshall 1996 *Astrophys. J.* **464** 760
- [87] W. Cui, S.N. Zhang, W. Focke and J.H. Swank 1997 *Astrophys. J.* **484** 383

- [88] B. Paul, P.C. Agarwal, A.R. Rao, M.N. Vahia, J.S. Yadav, S. Seetha and K. Kasturirangan 1997 *Astrophys. J.*
- [89] E.H. Morgan, R.A. Remillard and J. Greiner 1997 *Astrophys. J.* **482** 993
- [90] K. Ebisawa, Y. Ueda, H. Inoue, Y. Tanaka, and N. White, 1996 *Astrophys. J.* **467** 419
- [91] T. Oosterbroeck et al. 1996 *Astron. Astrophys.* **309** 781
- [92] N. Murray and J. Chiang 1997 *Astrophys. J.* **474** 91
- [93] N. Murray and J. Chiang 1998 *Astrophys. J.* **494** 125
- [94] J. Kormendy 1988 *Astrophys. J.* **325** 128
- [95] R. Bender, J. Kormendy and W. Dehnen 1996 *Astrophys. J.* **464** L123
- [96] R. Genzel, N. Thatte, A. Krabbe, H. Kroker, L.E. Tacconi-Garman, 1996 *Astrophys. J.* **472** 153
- [97] .R. Rao, P.C. Agarwal, B. Paul, M.N. Vahia, T.M.K. Yadav, J.S. Marar, S. Seetha and K. Kasturirangan, 1998, *Astronomy & Astrophysics* (in press)
- [98] M. Miyoshi and J. Moran 1995 *Nature* **373** 127
- [99] R.J. Harms, H.C. Ford, Z.I. Tsvetanov, G.F. Hartig, L.L. Dressel, R. Bohlin, G.A. Kriss, A.F. Davidsen, B. Margon and A. Kochhar 1994 *Astrophys. J.* **435** L35
- [100] S.K. Chakrabarti 1995 *Astrophys. J.* **441** 576
- [101] F. Macchetto, A. Marconi, D.J. Axon, A. Capetti, W. Sparks and Crane, P. 1997 *Astrophys. J.* **489** 579
- [102] G.A. Bower et al. 1998 *Astrophys. J.* **492** L111
- [103] R.D. Blandford and C.F. McKee 1982 *Astrophys. J.* **255** 419
- [104] K.M. Chang & J.P. Ostriker 1985 *Astrophys. J.* **288** 428

- [105] D. Kazanas & D.C. Ellison 1986 *Astrophys. J.* **304** 178
- [106] S.K. Chakrabarti & P. Bhaskaran, 1992, *Mon. Not. R. Astron. Soc.* **255** 255
- [107] S.K. Chakrabarti 1997 *Astrophys. J.* (submitted)
- [108] G.E. Eggum, F.V. Coroniti, J.I. Katz, 1985 *Astrophys. J.* **298** L41
- [109] T. Das and S.K. Chakrabarti 1997 *Astrophys. J.* (in preparation)
- [110] S.K. Chakrabarti 1986 in *Accretion Processes in Astrophysics*, (Eds.) J. Audouze & J. Tran Thanh Van, Editions Frontierès, Paris
- [111] S.K. Chakrabarti, L. Jin and W.D. Arnett 1987 *Astrophys. J.* **313** 674
- [112] J. Horgan 1988 *Scientific American* **258** 20
- [113] K. Arai and M. Hashimoto 1992 *Astron. Astrophys.* **254** 191
- [114] M. Hashimoto, Y. Eriguchi, K. Arai and E. Müller, 1993 *Astron. Astrophys.* **268** 131
- [115] B. Mukhopadhyay and S.K. Chakrabarti 1997 *Astrophys. J.* (submitted)
- [116] L. Jin 1990 *Astrophys. J.* **356** 501
- [117] I. Yi and R. Narayan 1997 *Astrophys. J.* **486** 383
- [118] S.K. Chakrabarti and B. Mukhopadhyay 1997 *Nature* (Submitted)
- [119] C.J. Hogan and J.H. Applegate, 1987 *Nature* **330** 236
- [120] E.L. Martin, R. Rebolo, J. Cesares and P.A.Charles 1994 *Astrophys. J.* **435** 791
- [121] F. Favata, G. Micela and S. Sciortino 1996 *Astron. Astrophys.* **311** 951
- [122] L. Jin, W.D. Arnett and S.K. Chakrabarti 1989 *Astrophys. J.* **336** 572
- [123] S.K. Chakrabarti 1996 *Phys. Rev. D* **53** 2901

- [124] S.K. Chakrabarti 1988 *J. Astrophys. Astron.* **9** 49
- [125] R. Genzel, N. Thatte, A. Krabbe, H. Kroker and L.E. Tacconi-Garman
1996 *Astrophys. J.* **472** 153
- [126] S.K. Chakrabarti 1996 in *Proceedings of the XVIIIth conference of the
Indian Association of General Relativity and Gravitation, IMSC report no.
117*

Figure Captions

Fig. 1a: Potential felt by photons in Schwarzschild space-time. Photons with impact parameter $b < 3\sqrt{3}$ would be swallowed by the black hole, while those with $b > \gtrsim 3\sqrt{3}$ escape to infinity.

Fig. 1b: Photon trajectories with near-critical impact parameter $b = 5.19615242$ at different radial distance x (measured in units of GM_{BH}/c^2). At each radial distance the conical volume is drawn with semi angle $\psi = \sin^{-1}[3\sqrt{3}/x\sqrt{(1 - 2/x)}]$. The shaded region is the ‘cone of avoidance’ and the unshaded region is the ‘cone of emergence’.

Fig. 2: Potential barrier of a Schwarzschild black hole as felt by incoming test particle with angular momenta $l = 0, 2, 2\sqrt{3}, 3, 4,$ and 5 (from bottom to top; in units of GM_{BH}/c). The dashed curve is the Newtonian potential drawn for $l = 2$ for comparison. Marginally bound and marginally stable orbit locations at 4 and 6 respectively (in units of GM_{BH}/c^2) are indicated.

Fig. 3: Evolution of accretion flow model that takes place every twenty years or so. Bondi flow (a), Keplerian disk (b) and the generalized advective disk (c) are shown. Beside each model typical spectrum is also shown in $\nu \log(F_\nu)$ vs. $\log(\nu)$ scale. In (c) variation of the spectra with viscosity (or, equivalently, relative accretion rates in the Keplerian and sub-Keplerian components is shown).

Fig. 4: Classification of the parameter space (central box) in the energy-angular momentum plane in terms of various topology of the black hole accretion. Eight surrounding boxes show the solutions from each of the independent regions of the parameter space. Each small box shows Mach number M against the logarithmic radial distance r (measured in units of $2GM_{BH}/c^2$). Contours are of constant entropy accretion rate $\dot{\mathcal{M}}$. Similar classification is possible for all adiabatic index $\gamma < 1.5$. For $\gamma > 1.5$, only the inner sonic point is possible other than an unphysical ‘O’ type point [5]. See text for details.

Fig. 5: Variation of shock locations with energy in accretion and winds for various specific angular momenta l (marked on curves). $a = 0.5$ is chosen. Segments marked a_3 and w_2 (solid curves) represent stable shocks in accretion and winds respectively. Other two segments (a_2 and w_3) represent formal shock locations which are unstable.

Fig. 6: Mach number variation (a-d) and angular momentum distribution (e-h) of an isothermal viscous transonic flow. Only the topology (a) allows a

shock formation in the steady flow. Transition to open (no-shock) topology is initiated by higher viscosity (α) or lower angular momentum (λ_{in}) or inner sonic point location (r_{in} measured in units of $2GM_{BH}/c^2$). These latter types produce nonsteady shocks [63]. In (e-h), flow angular momentum (solid) is compared with Keplerian angular momentum (dotted). The location from where the angular momentum is deviated varies with the three parameters. Figure is taken from Chakrabarti, [125].

Fig. 7: Ratios v_x/v_ϕ (solid) and densities (dashed) of three illustrative solutions of the advective flows [5]. Note that the centrifugal barrier close to the hole makes all the three solutions to behave in the similar way in the region $2 \lesssim x \lesssim 10 - 20$, emission from which strongly determines the spectral properties of the black hole. In a strongly shocked flow the variations in densities and velocities occur in a shorter length scale while in a weakly shocked or shock-free flows the variations occur in an extended region.

Fig. 8: Comparison of theoretical (solid) and numerical results in a one-dimensional accretion flow which may or may not allow a standing shock. Mach number (y-axis) is plotted against the radial distance (in units of $R_g 2GM_{BH}/c^2$). The long and short dashed curves are the results of the TVD and SPH simulations respectively while very long dashed curve is using explicit/implicit code. The curves marked ‘O’ and ‘I’ are for transonic flows which pass through the outer and the inner sonic points respectively. They are also reproduced perfectly with numerical simulations [62].

Fig. 9a: Ratio of disk angular momentum to the Keplerian angular momentum in a typical time dependent simulation in an advective disk. The plot is made after the steady state is reached. Note the deviation Keplerian disk at around $R \sim 30$. The flow becomes super-Keplerian close to the hole before becoming sub-Keplerian as it plunges in [62].

Fig. 9b: Numerical simulation result of a typical advective disk which forms a standing shock after deviating from a Keplerian disk. While the flow remains generally sub-Keplerian, a kink in the distribution at the shock is produced, which, however, remained stable throughout the simulation [62].

Fig. 10(a-c): Comparison of the schematic spectra F_ν vs. ν of a neutron star candidate (a: left panel) and a black hole candidate both in soft (b: middle panel) and hard (a: right panel) states. Neutron star spectra are composed of a multicolour black body component coming out of a Keplerian disk and a black body component coming out of the stellar envelop. In soft states a black hole shows a weak power-law component of a quasi-constant slope

(-1.5). In hard states the power law component is stronger and has a slope of ~ -0.5 .

Fig. 11: Spectral evolution of an accretion disk with a strong shock at $X_s = 10$ around a black hole of mass $3.6M_\odot$. The sub-Keplerian halo rate is $\dot{m}_h = 1$ and the Keplerian rates are marked on the curves. The dotted curve is drawn to include the effect of bulk motion Comptonization when $\dot{m}_d = 1$ [21].

Fig. 12: Typical spectral evolution of an X-ray nova. x_K (marked on the curves) could be very far away as in a low accretion rate, low viscosity disk. We chose: $\dot{m}_h = 1.0$ and $\dot{m}_d = 0.01$. Initially, at the onset of an outburst, the optical intensity goes up as x_K is decreased. Subsequently, the hard X-ray goes up first and then the soft X-ray is intensified. The $x_K = 9000$ and 8000 solutions resemble Novae spectra in quiescence [21].

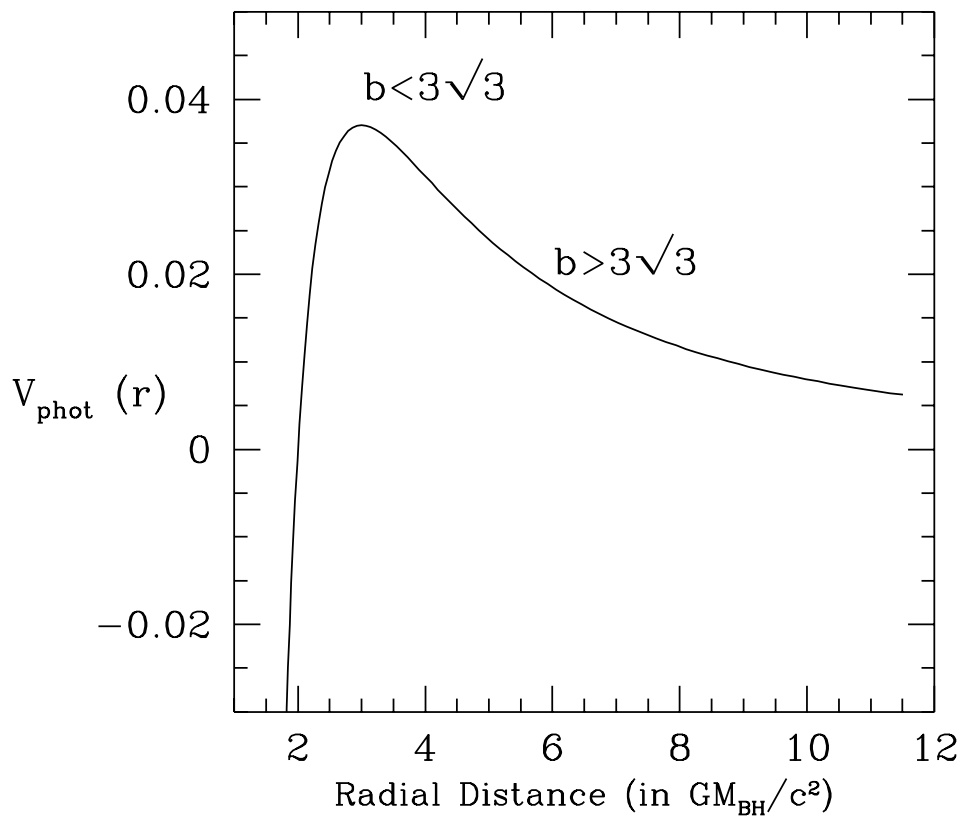
Fig. 13: Schematic diagram of the incoming and outgoing flows around a black hole. It is suggested that the CENBOL actually behaves like a stellar surface and causes the mass loss exactly in the same way the stars lose mass [107].

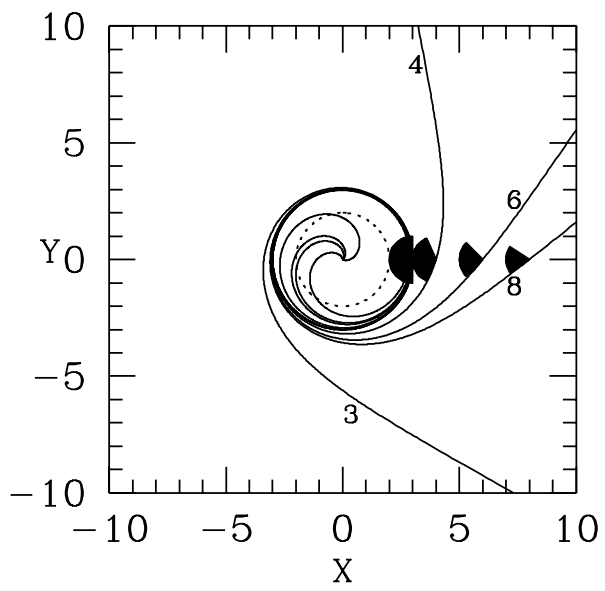
Fig. 14: Actual solution (Mach number along y-axis and $\log(r)$ along x-axis) of isothermal winds (dashed curves) arising of adiabatic accretion (solid) for a rotating flow with $\lambda = 1.89$ and $\mathcal{E} = 0.0038$ in presence of a centrifugal barrier at 18. Arrows indicate the direction of the outflow. Outflow rate is increased from bottom to top outgoing curves.

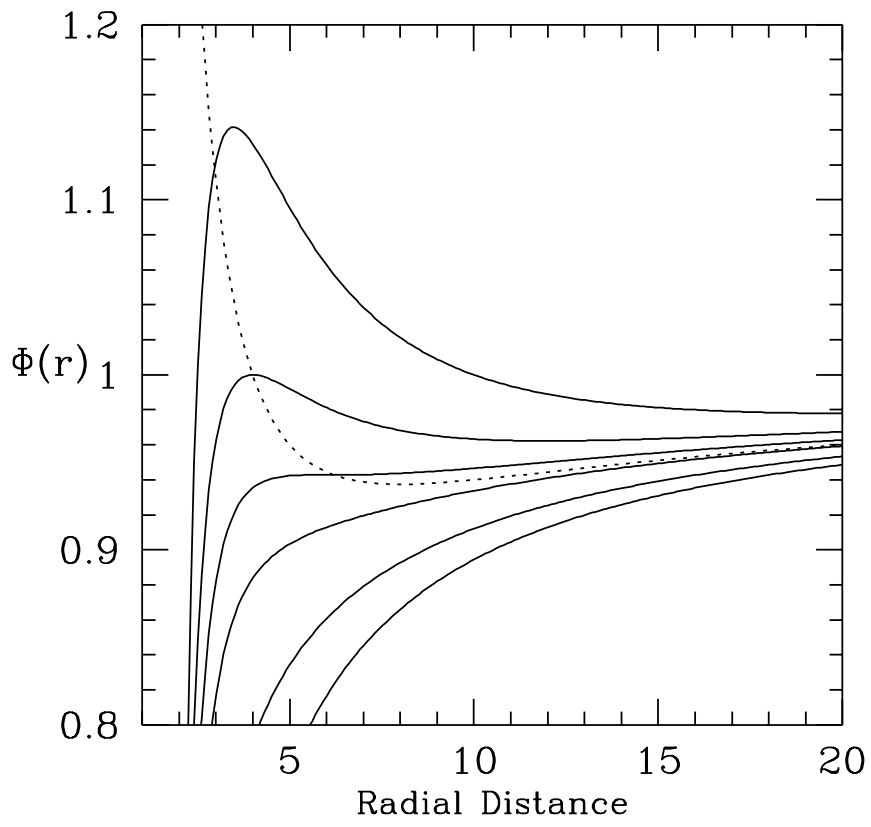
Fig. 15: Variation of the abundance as matter enters the advective disk regime. Here $10M_\odot$ central object and a mass accretion rate (sum of Keplerian and sub-Keplerian component) of $1\dot{M}_{Edd}$ is used. The cooling factor $f = 0.5$ and viscosity $\alpha_\Pi = 0.05$ were used which gave $x_K = 498r_g$. The shock is formed at $x_s = 13.9r_g$. The dotted curves are drawn when only the supersonic branch through outer sonic point is used, while the solid curves are drawn when the solution passes through both the sonic points and a shock.

Figure 16: Effect of the presence of an accretion disk on the gravity wave pattern in a binary black hole system consisting of two black holes with mass 10^8M_\odot and 10^6M_\odot . See text for the parameters used. In (a), the radial distance of the companion as a function of time are compared (dashed curve is with the disk, and the solid curve is without the disk), while in (b), the ‘chirp’ profile as function of real time are compared (profiles in the last few Schwarzschild radii are shown). When the sub-Keplerian disk is included, the

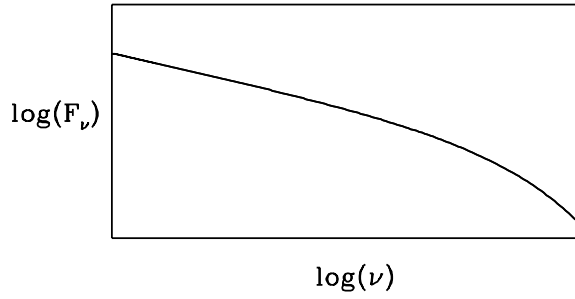
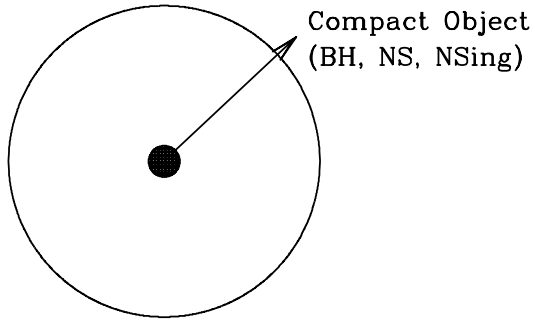
companion falls more rapidly due to enhanced loss of angular momentum.



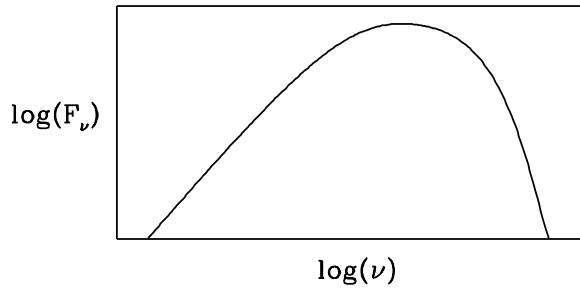
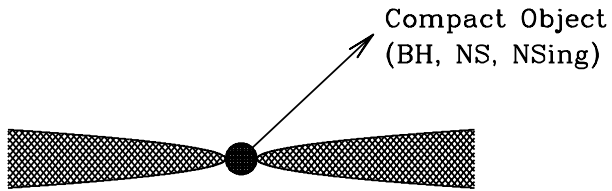




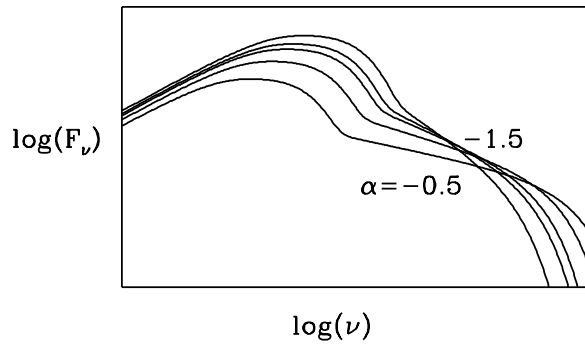
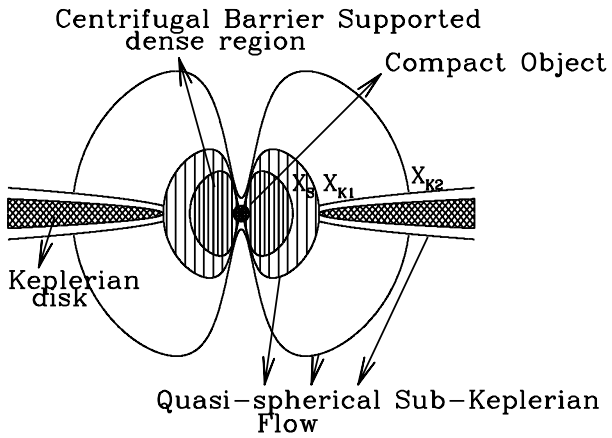
Bondi Flow (1950s)

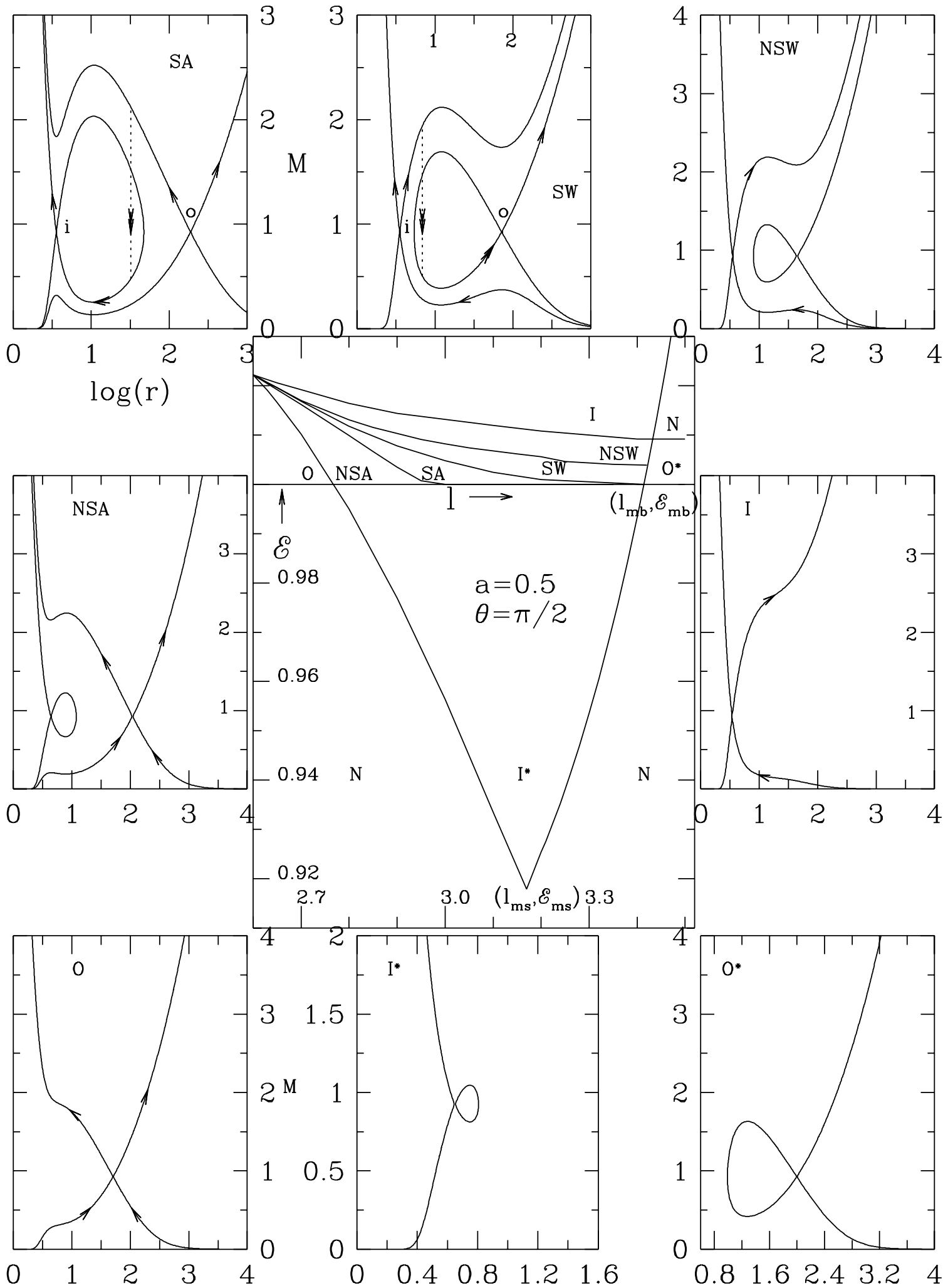


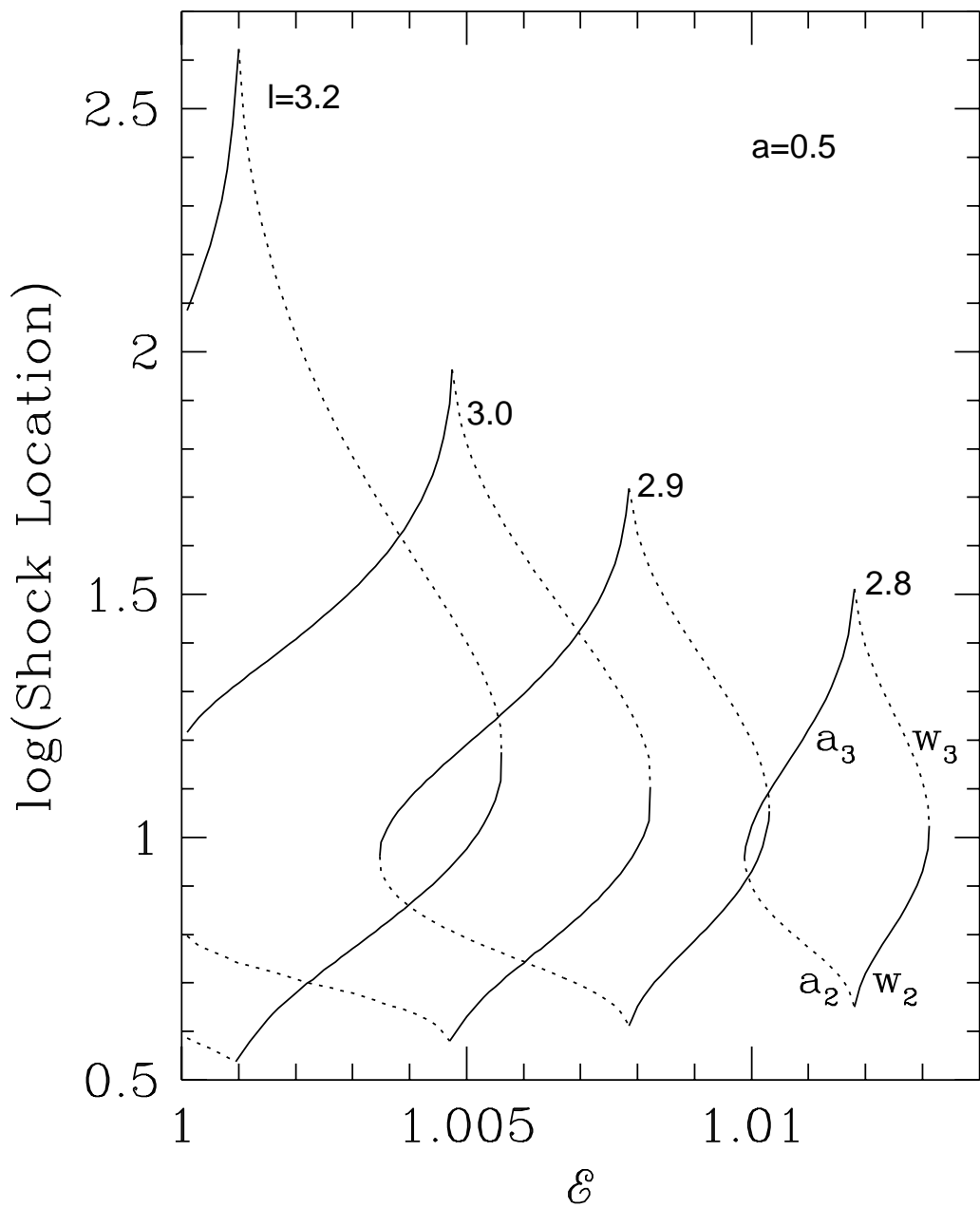
Keplerian Disks (1970s)

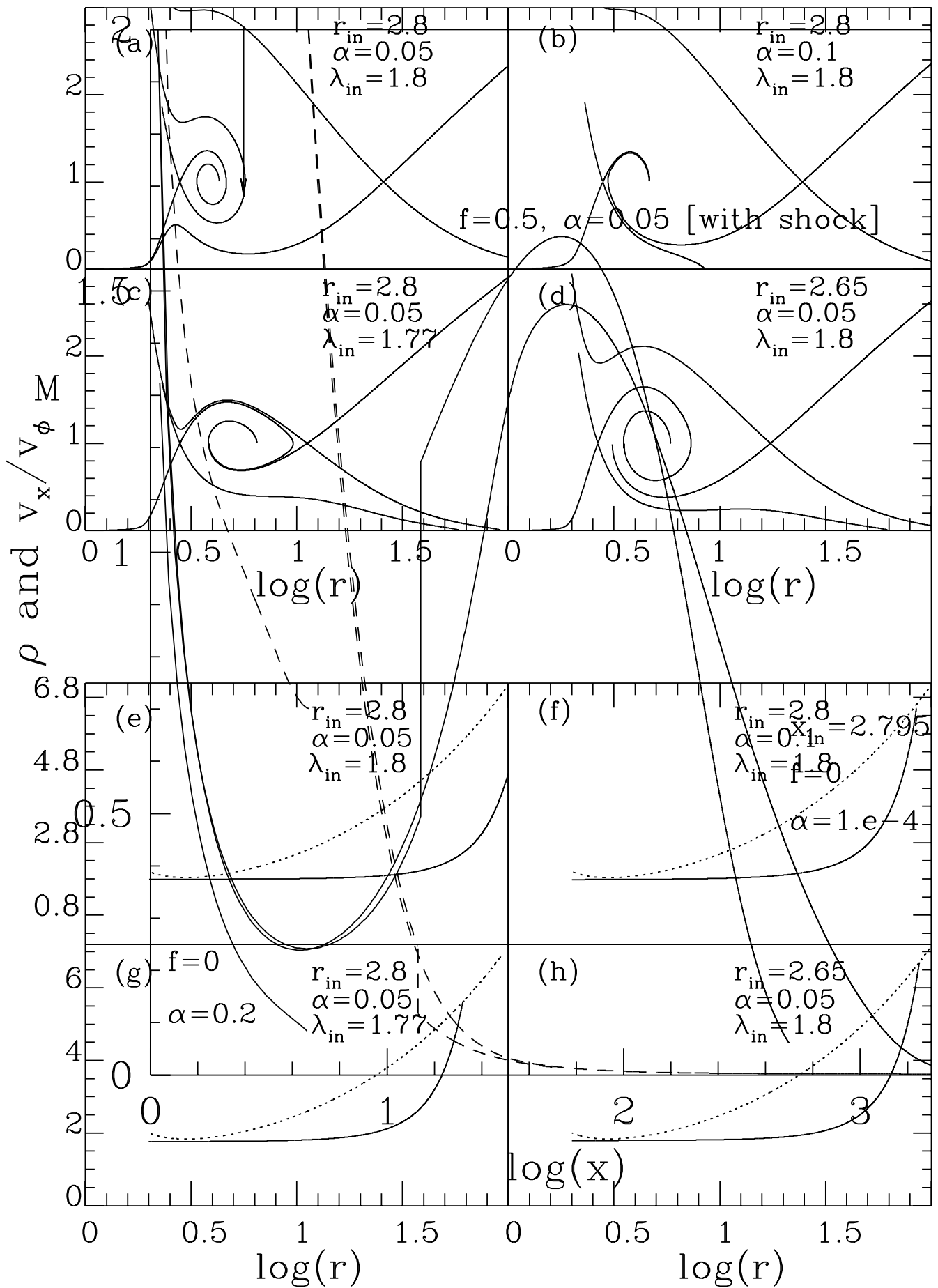


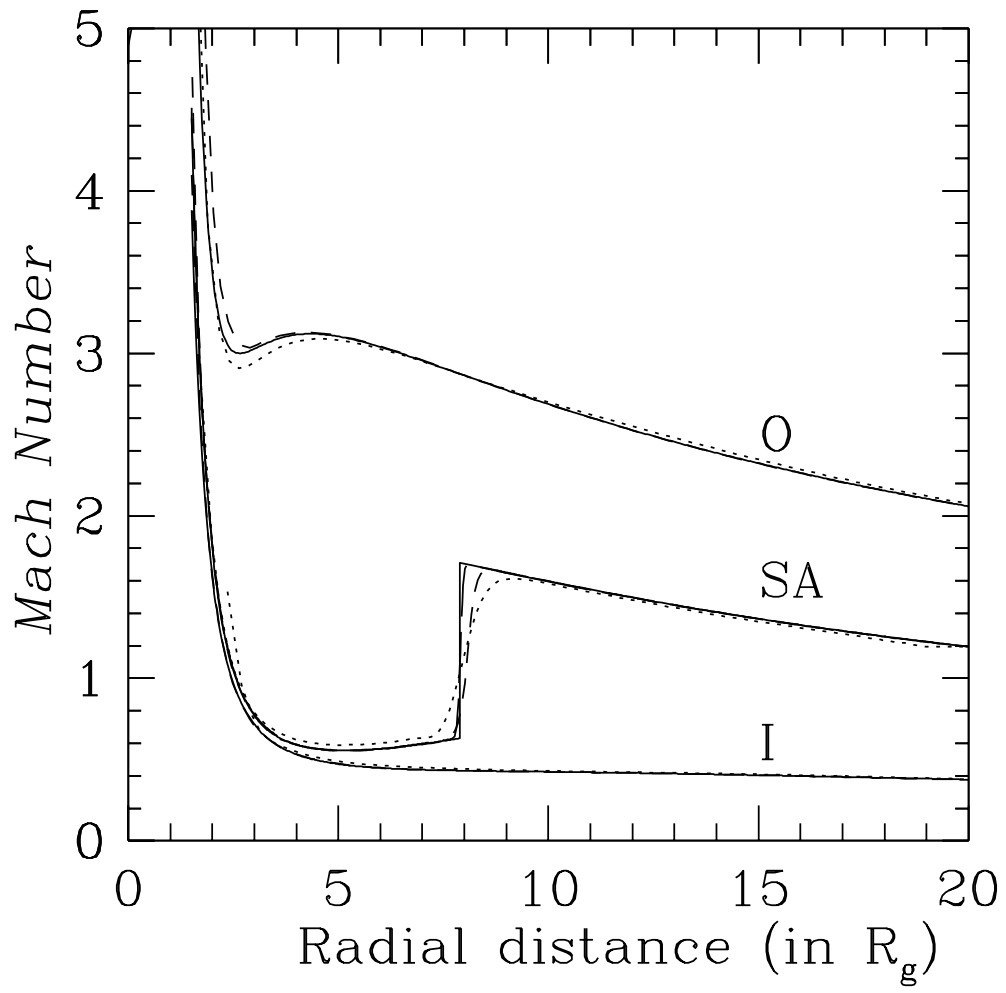
Advective Disks (1990s)

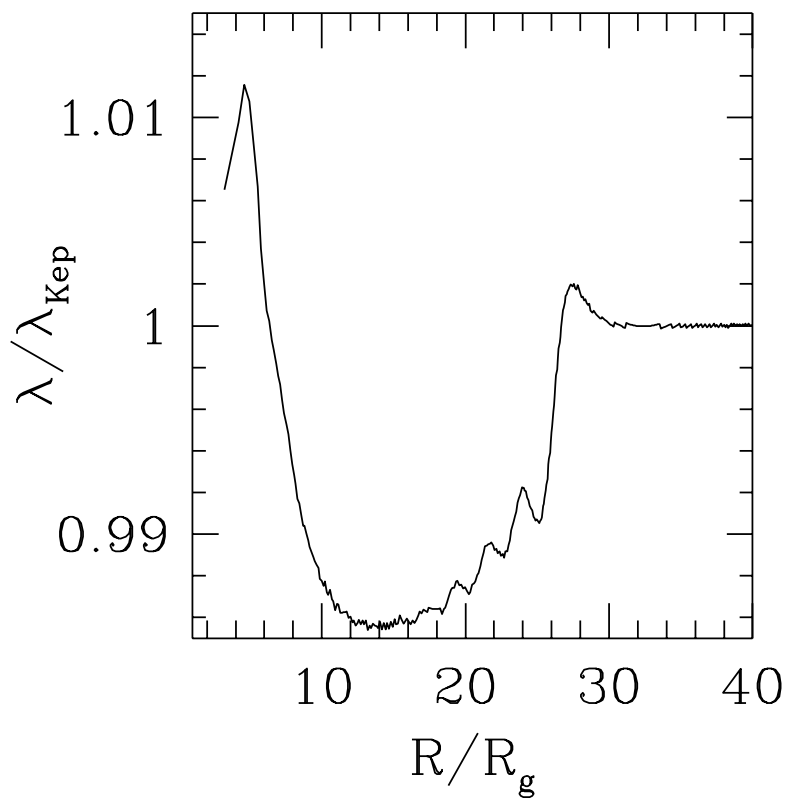


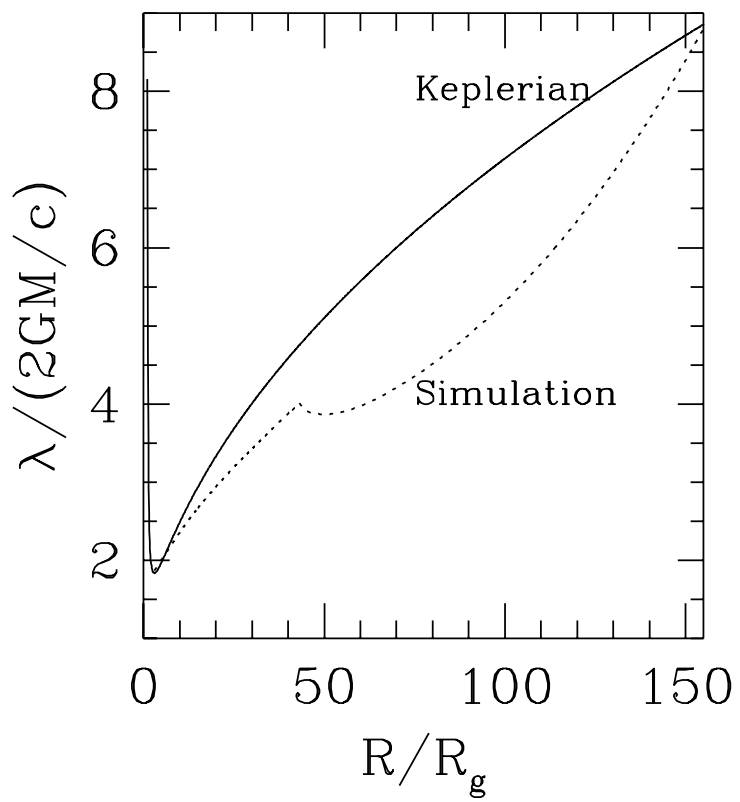


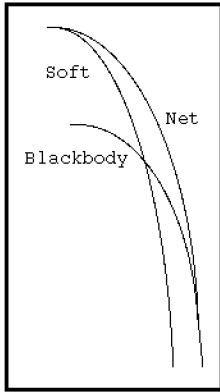




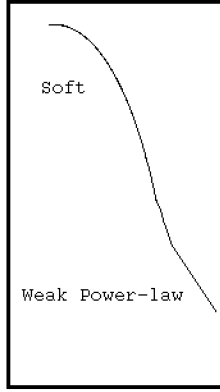




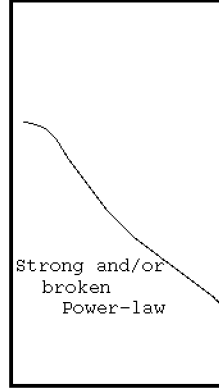




Neutron Star



Black Hole
(Soft State)



Black Hole
(Hard State)

